Department of Precision and Microsystems Engineering

On the efficiency of coupled vs uncoupled vibration energy harvesters under transient excitations

M.W. Wouters

Report no : 2021.006
Coach : T.W.A. Blad
Professor : J.W. Spronck
Specialisation : MSD
Type of report : M.Sc. Thesis
Date : 28-01-2021

On the efficiency of coupled vs uncoupled vibration energy harvesters under transient excitations

by

M.W. Wouters

to obtain the degree of Master of Science

at the Delft University of Technology,

to be defended publicly on 28 of January 2021 at 13:30.

Student number:	4585526	
Project duration:	September 2019 – Januari 2021	
Thesis committee:	Ir. J.W. Spronck,	TU Delft, PME
	Ir. T.W.A. Blad,	TU Delft, PME
	Dr. R.A. Norte,	TU Delft, PME

An electronic version of this thesis is available at `http://repository.tudelft.nl/`.

TU Delft

Preface

Before you lies the work which has emerged at the end of a long and twisting path. It is the end of my career as a student, but it also ushers in the rest of my life as an engineer. It was from a quite early age I realized I wanted to be a engineer, perhaps slightly influenced by my grandpa who was a very capable bicycle mechanic, and my dad who is an entrepreneur in metal construction. Always I wanted to 'look under the hood' so to say, see how something works or what drives a certain movement. This fascination has led me to choose most of the scientific programs in high school, and afterwards a higher education in Mechanical Engineering. After graduating on a very interesting project in the high-tech industry my supervisor encouraged me to continue studying on the next level, which led me to Delft and eventually towards this project in the Mechatronic system design group within the High-tech Engineering master track at TU Delft. My interests with understanding moving components and mechanisms perfectly line up with this research involving vibrations and resonating mechanisms. It was very fascinating to be able to work in this group with a group of people all working on similar projects and all working towards the same goal. I am very grateful I got the opportunity to follow my passion which led me to where I am today. Working in the Energy harvesting group has been a delight, although it was slightly derailed by a global pandemic in the middle of it. I wish the reader a lot of reading pleasure and hopefully he or she learns a thing or two.

M.W. Wouters
Delft, January 2021

Contents

1

Introduction

This chapter introduces the concept of energy harvesting, and later on vibration energy harvesting to the reader. The background, state-of-the-art technologies and principles are touched upon to provide a basic understanding of the topic such that the following research becomes more tangible and hopefully shows its importance to the general topic. It starts with general energy harvesting, followed by vibration energy harvesting which will be further specified in multi-modal vibration energy harvesting and offers a problem statement and research question. The thesis outline is shown in the end of this chapter.

Renewable energy has been a hot topic for some time now [34], as countries around the world are trying to decrease their dependence on fossil fuels. For large scale energy production the front runners in this category are solar power, wind energy and hydro power [2]. These installations all require big investments and complex infrastructure. For applications with a low power demand, locally, without a complex and expensive infrastructure behind it, small scale energy harvesting is a good alternative. Examples of this are a bicycle dynamo to power the lights on a bike, or a handheld flashlight with a crank which can be wound in order to charge the equipped battery. Another example is a mechanical, automatic wristwatch. The main difference between the wristwatch and the dynamo or flashlight is that the energy is not converted to electricity, but it is used to wind a coil which is used to drive the mechanism within the watch. The main element these examples have in common is that they are all small, mobile and require relatively low power.

(a) **Solar panel**

(b) **Hydro power installation**

(c) **Automatic movement of wristwatch**

Figure 1.1: **Examples of energy harvester systems in macro scale, and smaller scale [23],[1],[3].**

1.1. Vibration energy harvesting

Vibration energy harvesting is the act of scavenging energy present in ambient vibrations, and transducing that energy into other forms, electricity being the most common. These ambient vibrations can be observed in lots of different environments. Industrial processes like machinery operating at a certain frequency produce small amplitude, high frequency vibrations. Vibrations in the transport sector, like trains or trucks usually have a larger amplitude, but lower frequency vibrations. Then there's the human body, whose vibrations can also be used for energy harvesting. This can be done in the form of human motion, so for instance the walking motion where the impact of each footstep can be used. Or inside the human body, where heart contractions can be used to power an energy harvester. These stated examples all have wildly different values for amplitude, frequency and consistency. Because the source vibrations are so different from one another, the vibration energy harvesters are also different from each other. Generally speaking, VEHs are not plug and play. They are most efficient at certain very specific conditions, and are very sensitive to changing conditions which usually means their efficiency lowers dramatically when their operation conditions are not met. This means that for every application the source vibrations must be thoroughly analyzed and a VEH design must be chosen which is best suited for that specific application.

A VEH is a device that when placed in a environment where ambient vibrations are present, it will scavenge some of the energy present in these vibrations and transfer it to kinetic energy within the device itself. VEHs generally consist of three parts and can be approximated by a mass-spring-damper model. These three parts are: *Proof mass, Suspension and Transducer*.

The proof mass is a mass which captures the kinetic energy of the vibrations. It is the mass in the mass-spring-damper model, so as it starts to move due to the ambient vibrations it builds up kinetic energy which will later be converted into electrical energy. The suspension provides the restoring force for the proof mass. VEHs are of a limited size, so the kinetic energy, which only requires motion is transformed into a vibration by means of a suspension which acts as a spring in the mass-spring-damper model. In practice this can either be a conventional coil spring, or flexures which scale down better than coil springs or a magnetic restoring force can also be used.

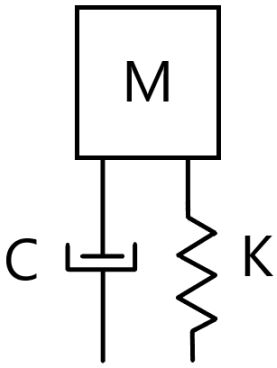

(a) **Schematic overview of mass-spring-damper model.**

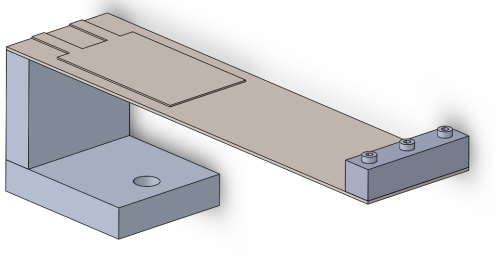

(b) **Rendition of cantilever, with simple cantilever connected through a base and with a proof mass attached to the end of the cantilever. Here the expansion represents a piezo-electric transducer.**

Figure 1.2

Transducer principles

The third part of the VEH is the transducer, which is the damper in the mass-spring-damper model. This part converts the energy from the kinetic to the electrical domain and also dampens the motion of the VEH. The measure of how well the transducer converts kinetic to electrical energy is called the coupling factor. The higher the coupling factor the more efficient the transduction process is. In a conventional hydraulic damper in a suspension system the dampened energy is converted to heat which is then lost to the surroundings, in a transducer in a VEH the dampened energy is what gets taken out of the system in the form of electric energy. This can be achieved in a number of ways, which all have their use cases in different systems. The three most used principles are: Piezo-electric, electromagnetic and electrostatic.

Piezoelectricity is a coupling between the electrical and mechanical domain which can naturally be found in certain crystals. A mechanical stress in the crystallic material is converted to an electrical charge. This can also be reversed, so if a electric charge is sent through the material a mechanical strain is induced in the material. Materials which exhibit the same phenomenon have also been developed which are more suited for use in practical applications. There are multiple ways piezoelectric transducers can be used in practice. in a micro-electromechanical system (MEMS) a piezoelectric layer can be incorporated in the material itself with electrodes also embedded into the material. On the larger scale a piezoelectric element is usually added after the manufacturing of the mechanism itself.

The electromagnetic principle is a coupling between, as the name says, the electric and magnetic domain. It is governed by Faraday's law of induction, which tells us that a change in magnetic field can produce a voltage in a conductive element. In practice this is most commonly found in electro motors. A permanent magnet is rotated in a conductor made of copper wires which produce a voltage in the wires. The same principle can also be used in a linear manner where the permanent magnet makes a linear motion instead of a rotating one. In energy harvesting it can be used in the linear way, but it doesn't scale down very well which means it is mostly used in larger applications.

In practice, and especially in small scale applications piezoelectric transducer seems to be given the greatest attention and is considered the easiest to work with and best performing transducer principle. [CITEER ERTURK]. Especially the fact that it is relatively easy to implement in a MEMS manufacturing process makes it viable to use in applications.

Applications

Vibration energy harvesters can be used in any situation where ambient vibrations are present. Examples of this can be an industrial process, automotive industry or medical devices. The advantage of using vibration energy harvesting in these cases is that the sensors can be entirely autonomous. No more battery maintenance has to be performed, which is an expensive enterprise in some cases. Or in some cases it can be dangerous, for example in pacemakers. In the state of the art pacemakers the battery has to be replaced every 10 years or so[20], this means that every 7 years an invasive heart surgery must take place which can lead to complications and is very expensive. Replacing the battery by a VEH eliminates the need for this surgery, leading to reduced health care costs and a decreases chance on complications on the use of pacemakers.

Research into vibration energy harvesting has been going on for some time . During the early years this has not gained much traction into real world applications, in part due to limited application possibilities and also poor performance. In recent years attention has grown for sensor networks, for use in maintenance, surveillance and sensing in industrial processes. These applications have in common that they use low power, and have a low duty cycle. Due to this increased attention and demand from industry, more research has gone into improving real world performance [9],[6],[22]. These research topics include amongst others; Frequency up-converter principle, non-linear generator research and multi-modal generator research. All these principles have one goal in common: Increasing power output over a wider range of frequencies.

1.2. Multi-modal vibration energy harvesting

For practical applications of vibration energy harvesting, multi-modal energy harvesters have a lot of potential because of their wideband power output. This means that the harvester is capable of generating significant power in a wider band of frequencies. A multi-modal generator is a VEH which has multiple distinct resonance modes. This is most commonly achieved by combining certain elements of the mass-spring-damper model in a way such that a system of VEH is created. Whereas a single mass-spring damper system can be described by the following equation:

$$M\ddot{x}(t) + c\dot{x}(t) + kx(t) = f(t) \tag{1.1}$$

For a multi-modal mass-spring-damper system this needs to be expanded to:

$$\begin{bmatrix} M_{11} & M_{12} \\ M_{21} & M_{22} \end{bmatrix} \ddot{\mathbf{x}}(\mathbf{t}) + \begin{bmatrix} c_{11} & c_{12} \\ c_{21} & c_{22} \end{bmatrix} \dot{\mathbf{x}}(\mathbf{t}) + \begin{bmatrix} k_{11} & k_{12} \\ k_{21} & k_{22} \end{bmatrix} \mathbf{x}(\mathbf{t}) = \mathbf{f(t)} \tag{1.2}$$

Where K is the stiffness (matrix), M is the mass (matrix), ω the eigenfrequency,x is the position (vector) and $f(t)$ is the forcing function of the system. This general equation can represent a wide range of different multi-modal systems depending on the matrix elements. Coupling, eigenfrequency, mode shapes and damping all depend on these system characteristics.

In figure 1.3a to 1.3c Different layouts of multi-modal VEHs are shown. Shown here are all two degree of freedom, coupled systems. More than two are degree of freedom systems also possible. As stated before, the transducers in a VEH are represented by the dampers, so in these three figures different layouts of transducers are shown. These different layouts make for different dynamic behaviour in the system. Eigenfrequency says something about steady-state cases. It says at what frequency the resonance modes are located, and the amplitude of the resonances is dependant on the damping ratio of the mechanism.

The VEH must be designed in a way such that power output is maximized. This means that the ambient vibrations must be analysed, and the resonance modes of the generator must match these ambient vibrations. However, even if the devices resonance modes are matched to the most prominent ambient vibration frequencies the output power can still be lower than can be expected if the device is slow to react to the constantly changing behaviour of the ambient vibrations. So the amount of times the source signal switches

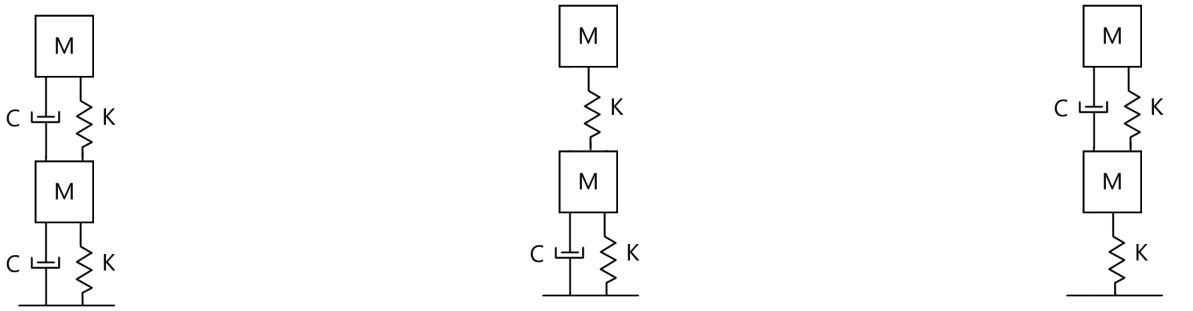

(a) **Two dampers**

(b) **One damper on bottom mass**

(c) **One damper on top mass**

Figure 1.3: **Three different iterations of a coupled system of multi-modal vibration energy harvesters**

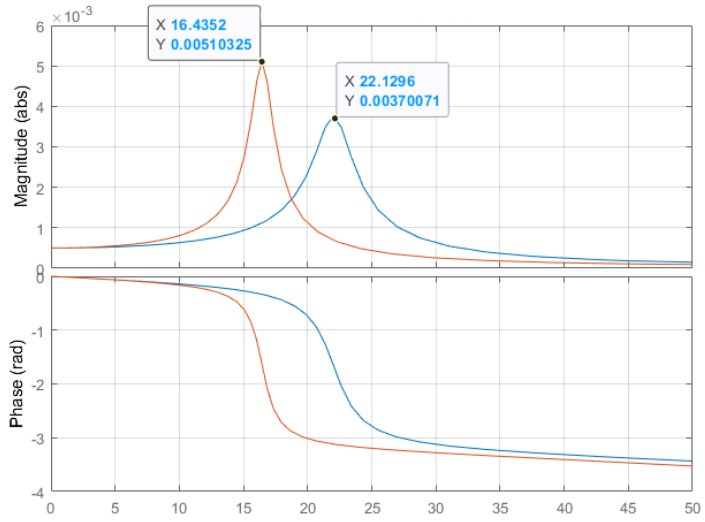

Figure 1.4: **Bode plot of an uncoupled double mass-spring-damper model.**

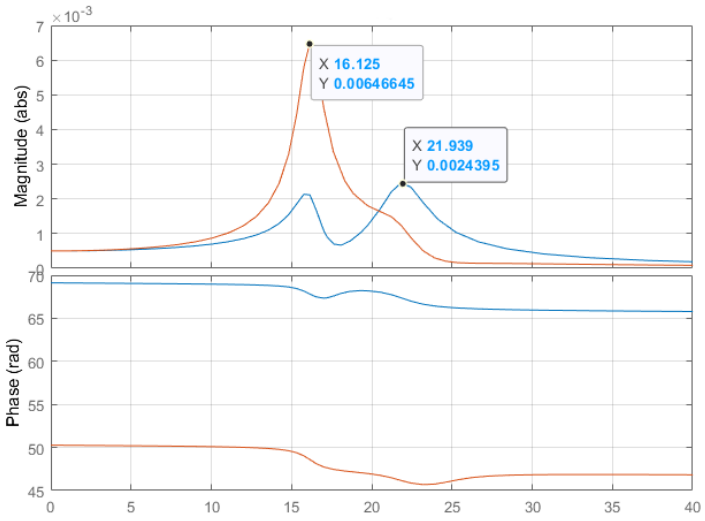

Figure 1.5: **Bode plot of a double mass-spring-damper model with coupling between the two masses.**

between prominent frequencies, or if frequencies are present at the same time can all influence the VEH power output, mostly in a negative way.

In this paper we will look into the dynamic behaviour of multi-modal vibration energy harvesters and how they deal with changing ambient vibrations, or more specifically the transients. In previous work a multi-modal vibration source is usually described by one of the two following equations: (source??)

A mechanism with finite, non-zero mass and stiffness always has a certain transfer function between input and output vibrations. If the mechanism has multiple modes and if these modes are coupled, there can be a substantial difference between the different cases.

The reason why looking at the dynamic behaviour of these mechanisms excited by transient vibrations is interesting is because it has a big influence on power output in real-world applications. It is also assumed there is a substantial difference in transient behaviour between VEHs with different layouts as shown in figure 1.3a to 1.3c.

This paper mostly focuses on finding out what entails good transient behaviour in VEHs, and what elements in a multi-modal VEH makes for good transient behaviour. This research can then be used to give recommendations such that in the future more efficient multi-modal VEHs can be designed for real world applications.

1.3. Problem description and Research objective

In theory multi-modal VEHs have a clear benefit in that they can give a substantial power output over multiple frequencies, which would increase the power output in real world applications with multiple dominant frequencies. However there is a discrepancy between testing a VEH in a lab under controlled circumstances, and applying a VEH in an environment with real-world vibrations. The presumption is that this discrepancy can be partly explained by the fact that real-world vibrations with multiple dominant frequencies constantly change between these frequencies and VEHs are not putting out maximum power instantly when they are excited by a resonance frequency. It is instead assumed that a vibrating mechanism always takes a few cycles to reach its full amplitude, which in the case of vibration energy harvesters means that transient phases in ambient vibrations cause a temporary drop in power output.The research objective is stated as follows:

In what manner do different types of multi-modal vibration energy harvesters react to transient behaviour in vibrations and to what extent does it reduce efficiency.

1.4. Thesis outline

The main focus point of this thesis is based on understanding transients in vibration energy harvesters. Several steps are addressed and shown in this paper. The second chapter is the literature study conducted at the start of this project. It focuses on multi-modal VEH and introduces a new performance metric. Also a classification into existing multi-modal VEH is shown there.

The next chapter is the main work of the thesis. In the same way as the literature paper, the main work is also shown in a short and concise manner. The thesis paper features a separate introduction to the work followed up by methods, results and a discussion.

A separate chapter features the results, conclusions and recommendations of the project in general. These results and conclusions are not pertaining to the work done, but offer more of a personal view and learning goals of the author.

Lastly the appendices are shown. To keep the thesis paper clear and concise, some work that was done was kept out of the thesis paper itself. These are added as an appendix. Appendix A features the model synthesis of the two models used in this research. Appendix B states the specifications of the equipment used. Appendix C shows a selection of results of the experiments conducted in this research to offer the reader an insight of how the power output results came about. Lastly Appendix D shows a sidetrack into Simulink modeling.

2

A new figure of merit to quantify performance in multi-modal vibration energy harvesters

The literature paper made in the literature study phase of this project is presented here. The paper starts with a problem description and essentially two different parts are presented. First a classification into different multi-modal vibration energy harvesters is shown, and then a new figure of merit to quantify multi-modal vibration energy harvester performance is shown.

A new figure of merit to quantify performance in multi-modal vibration energy harvesters

M.W. Wouters, T.W.A. Blad and J.W. Spronck

Abstract

Despite the fact that vibration energy harvesting has been an ongoing research topic for over two decades, the application of them in practice remains limited. One of the reasons for this is the big discrepancy between the improvement of performance of generators on paper, and the stagnating performance increases when applying generators to the real world. This is due to the fact that real-world vibration sources are rarely constant, instead they are changing in time due to a dynamic load case for example. For this reason more research has been done in wideband vibration energy harvesters (VEH), this paper specifically focusses on multi-modal VEHs. Multi-modal VEHs have multiple resonance peaks close to each other, making one larger bandwidth with significant power output. To characterize the performance of a single-mode VEH usually peak output power is reported, linked with parameters such as volume and mass of the generator. For multi-modal VEHs this is not sufficient, since it does not tell anything about bandwidth and shape of the frequency function. In this paper a comprehensive overview of multi-modal VEHs is shown to give the reader a clear idea of the work done in this field and how they all relate to each other. Furthermore, a figure of merit characterizing performance for multi-modal VEH, FoM_{MM} is introduced and tested against some state-of-the-art multi-modal VEHs found in literature. It is found that FoM_{MM} can be an excellent metric to assess performance of multi-modal VEHs and can be used as a guide to evaluate multi-modal VEHs in the future.

2.1. Introduction

The fast development and application of artificial intelligence in predictive maintenance, weather forecast and process optimization results in an increased demand in mobile sensors all around the globe. This also means that free mobility and wireless technology is of great importance because of its flexibility to be used in varying environments. With fast development in microelectronics and MEMS technology these sensors have a low energy demand and can be powered with very low power levels [21]. Vibration energy harvesters can fulfill this energy demand and thus also provide flexible wireless mobility.

Traditionally, applied VEHs consist of one degree of freedom (DOF) proof masses oscillating at the resonance frequency. The restoring force in these mechanisms can originate from a mechanical source, like a leaf spring, or a electrostatic source. The resonance frequency of the cantilever is the one which is most dominantly present in the application for which they are designed. However, in most practical applications there is a wide band of frequencies present and a cantilever operating at resonance frequency is quite inefficient when excited at a frequency different from its resonance frequency. This is mostly due to the high quality factor they are designed with to maximize output power. So the quality factor is a compromise between bandwidth and maximum power output. Multi-modal VEHs offer a wider bandwidth, meaning they offer power output at a broader range of input frequencies.

In recent years, a lot of research is done in wideband VEHs of varying types. Xiao [37] and Upadrashta [33] have presented excellent wideband VEHs in the form of an array of cantilevers. Toyabur,[31] and Bai, [4] have done work in multi-modal VEHs where multiple modes in a single body are exerted. All these papers present a frequency-power output graph; however, report on the performance in a different way. All these papers report on their performance in a different way, but all report a frequency-power output figure.

A challenge of these multi-modal generators is how to measure their efficiency and performance. Standard figures of merit (FoMs) do not suffice since they are usually a measure of peak power or -3db power bandwidth and do not offer any information about bandwidth, other than the first resonance peak or average power output over the bandwidth. The goal of this paper is to introduce a new figure of merit specifically suited for

assessing the performance of multi-modal wideband VEHs.

First a comprehensive mapping of available multi-modal VEHs is shown in section 2. Then more traditional FoMs are analyzed in the next section, subdivided in general metrics and ones specifically designed for wideband VEHs. In section 3, a new, more suited FoM is presented and, a variety of different multi-modal generators found in literature is subjected to this FoM in section 4 and shown in an overview. Lastly the discussion is presented in section 5 and the conclusions are drawn in the last section.

Applications

Energy harvesting generators can be viewed as a very wide range of different techniques. However, in this review we look solely at vibration energy harvesters using compliant mechanisms, because they are most often used in practice. They are small in footprint and if used in the right environment can act as a very robust power source.

VEHs are especially useful in remote or hazardous environments, where it is expensive or impossible to have a connection to the power grid and dangerous or expensive to do maintenance (replacing the battery). In environments where the frequency of the ambient vibrations is known and does not fluctuate a lot, for instance like train tracks or vibrations of a controlled industrial machine always operating at the same frequency, a single-mode VEH operating at the resonance frequency is the best solution and offers the best power output [25].

However, in environments where the ambient vibrations are somewhat unknown or constantly changing due to a change in temperature for example a single-mode VEH will perform badly because the power output drastically decreases as the input frequency deviates from the resonant frequency of the device. This can be seen in figure 2.1. Due to the high quality factor of single-mode VEH the bandwidth is very small. A wideband VEH is more suited on this case because it uses the power contents of the source excitation more efficiently.

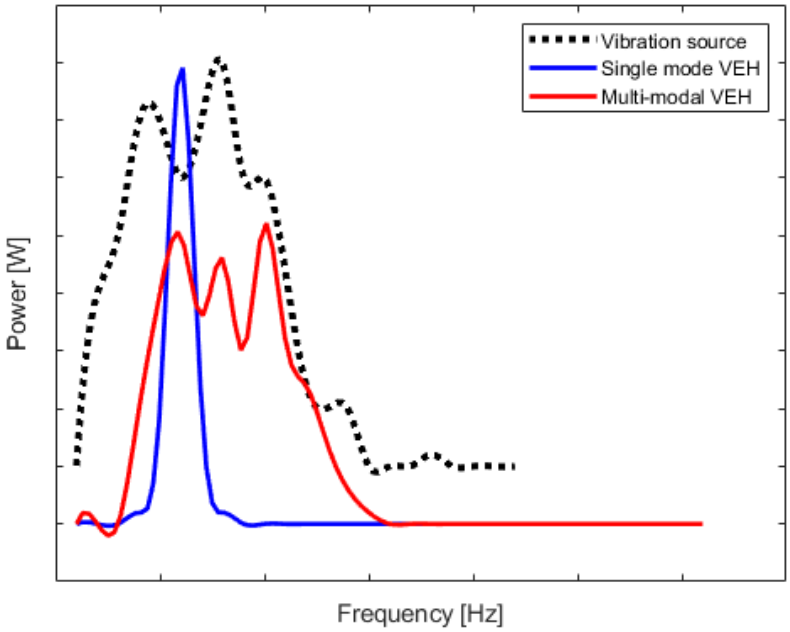

Figure 2.1: **Power contents of an imaginary vibration source in black, with a made-up single-mode VEH characteristics in blue and made up multi-modal VEH characteristics in red.**

In the real world, vibration sources rarely consist of only one or two dominant frequencies with a small bandwidth and without the presence of noise. Actual vibrations vary with varying parameters such as load case, wear, temperature etc. In figure 2.1 the case of a car driving on suburban roads can be seen. The actual vibrations depend on the speed of the car, the stretch of road the car is driving on, and the number of passen-

gers and luggage aboard the car. Also shown in figure 2.1 are two different imaginary VEH, one single-mode and one multi-modal. Both have their resonance peaks inside the high energy spectrum band of the vibration source. However, since the multi-modal VEH has three peaks of similar magnitude as the single-mode version, its total power output is significantly higher over the total spectrum. Since the total spectrum is addressed during a ride, this yields a higher total energy and thus a more consistent power supply to the device the VEH is powering. So in this particular case with a vibration source with significant power content over a wide spectrum, a multi-modal VEH trumps the single-mode version.

Figure 2.2 shows a mapping of all the multi-modal VEHs based on compliant elements found in literature. This review focuses on VEHs based on compliant elements because most of the work done features compliant elements in some way. When directly comparing different generators with each other it is important that all of them are based on the same principle to make a even comparison. First the three most important multi-modal systems are explained in text, then a comprehensive overview of all available multi-modal systems subdivided in a logical manner is shown.

2.1.1. Multi-modal classification

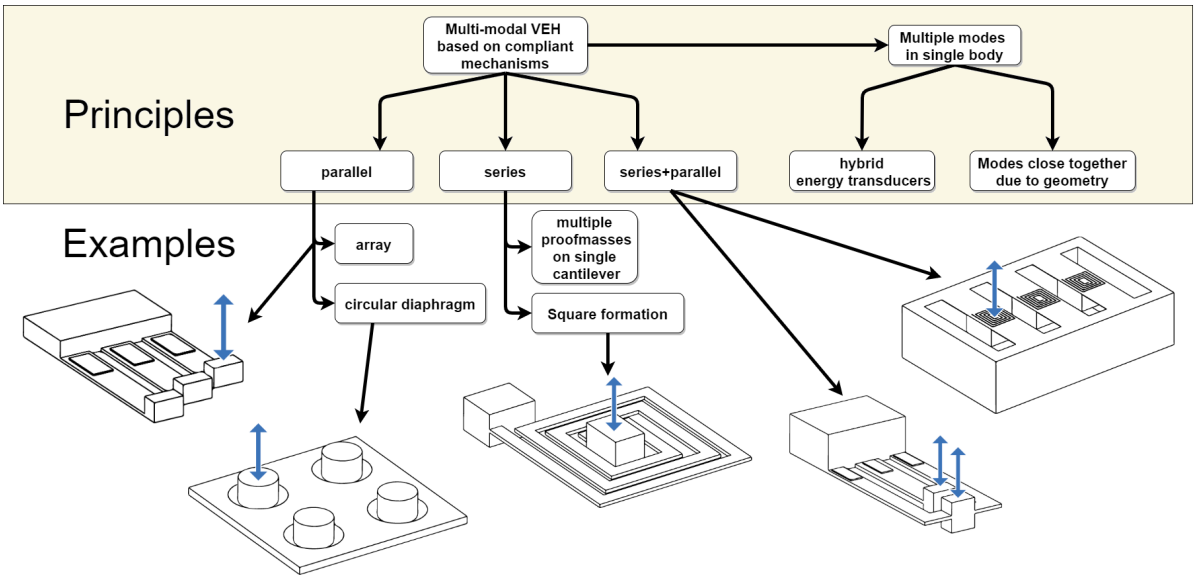

Figure 2.2: **Comprehensive overview of multi-modal VEH. Also shown are examples of specific applications based on generators found in literature.**

- Hybrid energy harvesting [30]

  To achieve a wideband energy harvesting system, a combination of transducers can be used. For example both an electromechanical and a piezoelectric transducer can be implemented in the generator. Since these transducers add damping and/or stiffness to the system, but have different characteristics, they effectively tune the resonance frequency of the mechanism and can thus make the output power more substantial in a wider bandwidth. [8],[19].

- Array of cantilevers [27]

  In a VEH the goal is often to match the first natural frequency of the mechanism to the most dominant frequency of the source vibration. The first eigenfrequency of a cantilever is dependent on the geometry and material properties according to equation 2.1 and 2.2.

$$\omega = \sqrt{\frac{k}{m}} \tag{2.1}$$

Where k is the stiffness and is governed by equation 2.2.

$$k = \frac{3EI}{L^3} \tag{2.2}$$

Here we can see the stiffness is dependant on both the material and the geometric properties.

To make a wideband VEH, an array of cantilevers of varying geometry can be used with increasing first eigenfrequency. This is most easily achieved by increasing the length or the thickness of the cantilever, since the length and thickness have a cubic term in the stiffness equation. If these resonance frequencies are sufficiently close together, this ensures that within a certain bandwidth substantial power can be drawn from the device. One more advantage of this system is that there are multiple proof masses present. So the dynamics of one cantilever and proof mass combination do not influence the dynamics of the other ones. A disadvantage of this type of system is that for a comparable volume and mass, the separate proof masses are smaller and lighter than a counterpart with only one proof mass, which means the maximum power output is also decreased.

- Exciting multiple DOF in single body with single proof mass, [12]

  Naturally a cantilever with a proof mass has multiple DOF. It has natural frequencies in all three major axes and also rotational DOF. Usually, the resonance frequency along the length axis is much lower than the other eigenfrequencies due to the slenderness with which these elements are designed. However it is possible to design the geometry parameters of an element in such a way that the eigenfrequencies of two DOF are rather close together such that they can both be used in a VEH to expand its usable bandwidth [12].

- Flexures in a combination of series and parallel

  By far the most work done in research contains some form of combination between flexures both in parallel and in series. A lot of creative designs can be made when these combinations are used, as demonstrated by [11] and [29]. Usually these generators have only one proof mass, but due to their geometry, different eigenmodes are excited at different frequencies. These usually involve a translating and rotational mode.

The four principles listed above is what most work found in literature is based on. Figure 2.1 shows an overview of all multi-modal VEHs found in published work. The types of generators shown in the overview but not listed in the classification show close resemblance to the ones listed in the classification. Therefore, it was decided to keep the classification as compact as possible.

2.2. Figures of merit for vibration energy harvesters

Judging performance in VEHs is not a trivial task. The most obvious metric would be the peak output power since that is the purpose of the device. However, just mentioning peak output power does not cover all the bases, even less so for multi-modal VEH. One of the goals of a FoM is to be able to directly compare two or more different VEHs. In order to do this, more properties of the generator need to be taken into account. Mass and volume first come to mind. Scaling the volume of a generator has a cubic effect on output power and a heavier proof mass means more energy is put into the generator for a given excitation. Some relevant figures of merit are discussed next.

The general FoMs like normalized power density (NPD) and Volume figure of merit (FoM_v) are intended for linear generators with one peak of resonance. However, some parts of these FoMs can be used for the FoM introduced later, for that reason the relevant parts will be stated here.

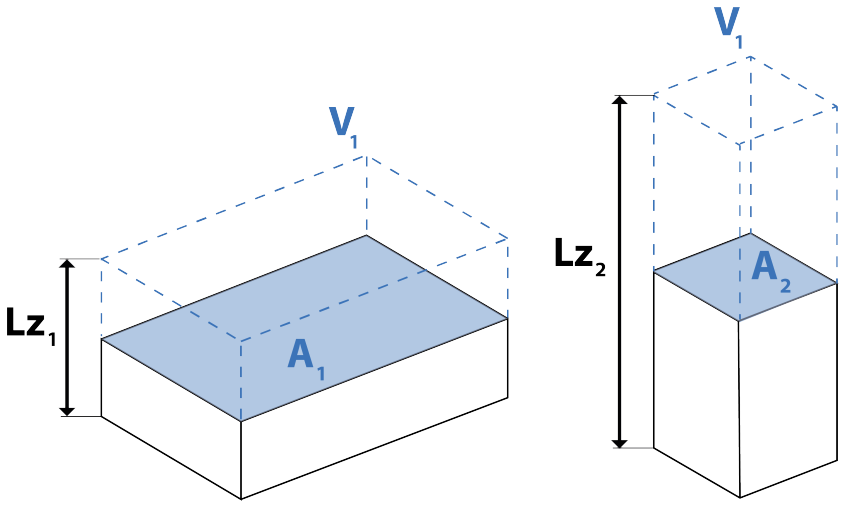

Figure 2.3: **Two imaginary generators with the same volume and mass. The second generator is potentially capable of producing more power due to a larger dimension in the moving direction.**

Generator figure of merit

In [7], Blad proposed the generator figure of merit, which is a variation of the FoM_V proposed by Mitcheson [21]. The main difference between the FoM_V and FoM_G is that the $V^{\frac{4}{3}}$ term in FoM_V is replaced by VL_z in FoM_G where L_z is the dimension in driving direction. This term accounts for the fact that a longer dimension in driving direction enables a higher efficiency. So this metric accounts for weight, volume and shape as well as the input signal. Also the density of the proof mass which was previously stated in gold is now replaced by the actual density of the material used, because while gold would be a preferred material for the proof mass due to its high density, it makes more sense to use the density of the actual material of the proof mass since gold is not always the most suited material for a variety of reasons.

$$\eta = FoM_G = \frac{P}{\frac{1}{16} Y_0 \rho_M V L_z \omega^3} \tag{2.3}$$

Where Y_0 and ω are the amplitude and frequency of the driving motion, respectively. V is the total volume of the generator and L_z is the driving motion, as can be seen in figure 2.3.

The previously mentioned figures of merit are all excellent ways to judge performance for VEHs in their own right. However, all of them only offer insight for linear single-mode generators since they all look at peak power output and disregard the number of resonance peaks, let alone any bandwidth widening effects that come with it. To properly judge performance for a multi-modal VEH, these figures of merit are insufficient; for that reason, a new figure of merit will be introduced in the next section specifically tailored for multi-modal VEHs.

Wideband figures of merit

In the next section, two figures of merit are introduced specifically to assess wideband VEHs are mentioned and analyzed. Since the new FoM introduced in this paper is also for wideband VEHs, some elements of these FoMs are also used in the new one.

Bandwidth figure of merit

In [21], Mitcheson introduced a new figure of merit called Bandwidth figure of merit. For this FoM he took the FoM_V introduced by himself and added bandwidth information. For this he used the -1 dB bandwidth

instead of the more widely used -3 dB bandwidth because it gives greater credit to generators with flatter frequency responses.

$$FoM_{BW} = FoM_V \times \frac{\delta\omega_1 dB}{\omega} \tag{2.4}$$

Where FoM_V is the volume figure of merit, which is a figure of merit based on the mass, volume and also amplitude of the excitation.

Systematic figure of merit with bandwidth information

In [18], Liu introduced the $SFoM_{BW}$ found in equation 2.5.

$$SFoM_{BW} = E_{HW}\left(\frac{\Delta f}{f_c}\right)Q_m\rho_{eff} \tag{2.5}$$

Where E_{HW} is the effectiveness redefined for wideband VEHs, $\frac{\Delta f}{f_c}$ is the bandwidth normalized by the center of the band, Q_m is the quality factor of the mechanism and $\rho_{eff} = \frac{M}{V_{tot}}$ is the effective mass density, not only that of the proof mass but of the whole generator.

For the effectiveness figure, Liu [18] has decided to use the average power over the region he is observing instead of the peak power in that region.

$SFoM_{BW}$ is the only figure of merit found in literature specifically made for wideband VEHs. It is an excellent FoM for wideband VEHs but some some parameters are accounted for more than once, like mass and volume are both in E_{HW} and in ρ_{eff}. And also the fact that the quality factor has a positive correlation to the FoM is a peculiar choice because it has a direct effect on power output, which is already accounted for in E_{HW}.

2.3. Introducing new FoM for multi-modal VEH

For linear single-mode VEHs, efficiency is a good metric, which also takes into account volume, mass and the vibration source. For linear multi-modal VEH, bandwidth and average generator efficiency in that bandwidth region is a better metric to gauge how much power can be drawn from a certain vibration source. Using these elements a new figure of merit is proposed here, called the multi-modal figure of merit.

$$FoM_{MM} = \left(\frac{\Delta f}{f_c}\right) \times \int_{f_{lb}}^{f_{ub}} \eta d\eta \times \left(\frac{\eta_{avg}}{\eta_{max}}\right) \tag{2.6}$$

Where FoM_G is the generator figure of merit introduced by Blad, [7]. $\frac{\Delta f}{f_c}$ is the bandwidth where f_c is the center frequency and Δf is the band of frequencies bounded by the half efficiency limit on both the lower and upper bound of the efficiency-frequency curve as can be seen in figure 2.4. The integral of η_{peak} is bounded by the same bounds and is a measure of the average efficiency, and thus also average power output across this region of interest.

Figure 2.4 gives a visual representation of some of the elements used in FoM_{MM}. The definition of the bandwidth is given by $\frac{\Delta f}{f_c}$, where Δf is defined by the two dotted lines which represent the half efficiency boundaries. Meanwhile the center frequency f_c indicated by the dashed line is the average frequency between the half-efficiency points. The efficiency is used instead of the power because it is a more inclusive metric than power since it takes into account mass and volume specifications of the generator.

Next, the integral of the efficiency is defined in figure 2.4 as the shaded region. This integral sums up the efficiency of the generator in the region of interest where a significant amount of power is generated. This

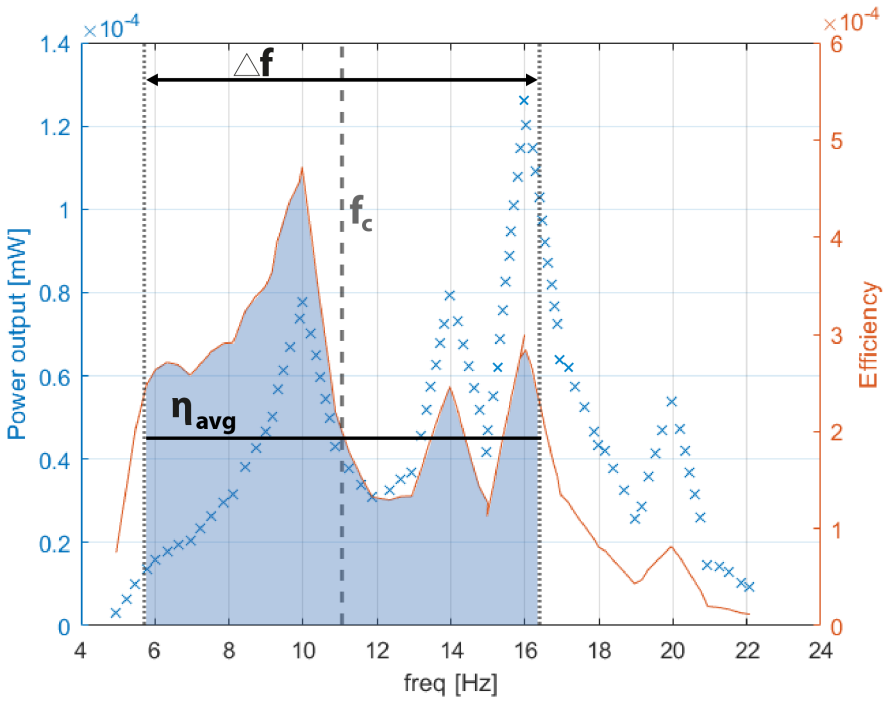

Figure 2.4: **Frequency-power plot of VEH by Toyabur [32] on the left y-axis, and frequency-efficiency plot on the right y-axis. The area in blue represents the integral of the efficiency bounded by the -3 dB efficiency points. The vertical solid lines represents the average efficiency over the bandwidth.**

integral is a measure of the efficiency in this region and as can be seen it has a positive correlation to power output in the region of interest. A higher value for the integral means a higher average efficiency and thus more power output.

As a metric to assess the overall performance of the design of the VEH, FoM_G is used since it takes into account all of the relevant design parameters of the generator. Not only mass and volume, but also the shape of this volume is addressed and thus FoM_G gives a very clear idea of the efficiency of the generator.

The last term in FoM_{MM} is the average efficiency normalized by the peak efficiency. If this term was not present in the FoM a very big bandwidth would compensate for a very low average efficiency. So an almost flat region of interest capped by two efficiency peaks would generate a high value for FoM_{MM}. Introducing the average efficiency in the figure of merit nullifies this effect and thus a high average efficiency with reasonably high bandwidth.

The FoM_{MM} provides a better measure for the performance of multi-modal VEH than the FoMs mentioned in the previous section because it is the only one which contains a measure of how much energy the generator is capable of putting out in a certain region of interest, encapsulated in $\int_{f_{lb}}^{f_{ub}} \eta_{peak}$. This integral sums up the efficiency of the generator in the region of interest. So the bigger the bandwidth and the higher the efficiency the bigger this figure is.

2.4. Results

The FoM_{MM} is specifically created to assess performance of multi-modal VEHs. To gain some insight as to how this FoM_{MM} relates to other wideband FoMs we apply some multi-modal VEHs found in literature to the new FoM_{MM} and other FoMs.

Since an extensive set of data, including a frequency-power curve is needed to deduce bandwidth, a rather small set of papers qualify to perform this test on. However, a set of ten generators has been found to have

Name	Type	Volume $[mm^3]$	NPD $[kgsm^{-3}]$	FoM_v	FoM_G	$SFoM_{BW}$	$FoM_{MM}[Hz]$
Bai [4]	1 proof mass	11664	0.025	0.151	0.527	0.003199	0.067
Gong [10]	1 proof mass	$7.7 * 10^3$	0.167	0.866	0.463	0.006272	0.010
Liu [16]	1 proof mass	35	$6 * 10^{-6}$	$3 * 10^{-5}$	$7 * 10^{-5}$	$2.7 * 10^{-07}$	$3.38 * 10^{-5}$
Liu [17]	1 proof mass	32	$1 * 10^{-9}$	$2 * 10^{-7}$	$6 * 10^{-7}$	$6.6 * 10^{-10}$	$4.52 * 10^{-7}$
Ramirez [24]	1 proof mass	11000	0.002	0.023	0.088	0.000084	0.003
Su [28]	Array	11760	0.017	0.444	1.473	0.001502	0.580
Toyabur [31]	1 proof mass	27000	$3 * 10^{-7}$	$6 * 10^{-6}$	$4 * 10^{-5}$	$4.2 * 10^{-08}$	$1.73 * 10^{-5}$
Upadrashta [33]	Array	12480	0.009	0.130	1.269	0.0016	0.001
Kim [12]	1 proof mass	88000	$3 * 10^{-6}$	$9 * 10^{-6}$	$7 * 10^{-6}$	$1.70 * 10^{-07}$	$7.81 * 10^{-7}$
Xiao [37]	Array	96040	0.973	2.295	3.962	0.134	0.479

Table 2.1: **Basic design parameters and performance metrics for different multi-modal vibration energy harvesters found in literature.**

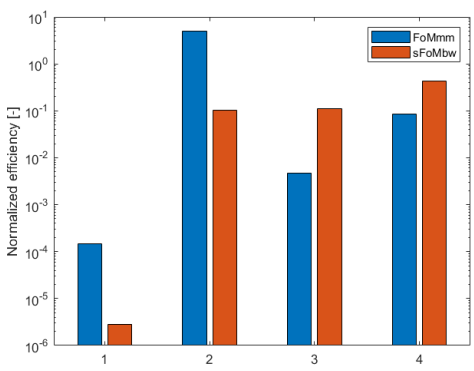

(a) **Comparison between FoM_{MM} and $sFoM_{bw}$ for a number of generators.**

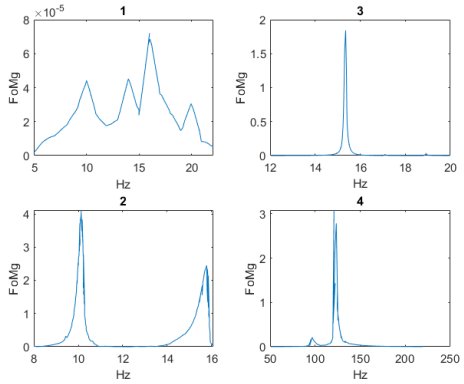

(b) **Frequency response function of a number of generators corresponding to the bar plots in figure 2.5a.**

Figure 2.5

enough data to be able to fill in all the relevant figures of merit. In table 2.1 these generators and their relevant parameters and their respective values to the FoM_{MM} are shown.

Out of the data in table 2.1, the two wideband FoMs are most interesting to directly compare. To that end the values for FoM_{MM} and $sFoM_{bw}$ are normalized against their mean value and then their values are plotted against each other for every generator. A selection is made for a number of generators which show a clear division between ones that show a better relative value for FoM_{MM} and ones that are better in $sFoM_{bw}$, this is plotted in figure 2.5a. Their respective frequency response functions are plotted in figure 2.5 to show the clear difference between their behaviour.

2.5. Discussion

Not enough papers have been found supplying enough data to be able to make a real distinction between different types of multi-modal VEHs. So nothing conclusive can be said about how different types of multi-modal VEHs found in figure 2.2 relate to each other in terms of performance. However, a trend can be observed between the different figures of merit the generators are tested against.

A wide spread in FoM_{MM} between different generators can be observed. It is not very evident which part of the input parameters is mostly responsible for this. Diving into the numbers however shows that some generators report really bad power output numbers compared to their counterparts. It should be noted that the reporting of parameters like volume especially, is quite inconsistent. So for some of the data used in this paper the volume figures are deducted from figures and tables. A reason for this is that some authors have

different definitions of volume with relation to energy harvesters than other, for some it is the minimally used volume by flexures and proof mass, others report the minimally enclosed cubic volume which is usually much bigger.

Multi-modal VEH mapping

The mapping presented in this paper is designed to be all inclusive. The starting point is chosen to be vibration energy harvesters which employ compliant mechanisms, flexures in most cases, in some way. The reason for this starting point is that it makes for a fair starting ground since they all follow the same basic principles. A generator which relies on electrostatics for its restoring force has different governing equations and uses volume in a radically different way, so testing it against the same figures of merit would clearly be advantageous to one or the other.

All the generators found in published research were looked at fundamentally in order to understand the kinematics. All of the different types of VEHs shown in the map have at least one example found in literature, but some of them have much more. It is found that most examples can be found in the form of an array of cantilevers, and a combination of series and parallel flexures. It is possible to make a further division in the map after some of the types shown in the figure, especially for the combination of series and parallel a lot of different architectures can be found. However it was found that they all fundamentally look alike and was thus not needed.

Figures of merit

Most of the work done in figures of merit and benchmarking in VEHs is done for linear single-mode generators. The $SFoM_{BW}$ is the only figure of merit found in literature made specifically for wideband VEHs. In contrast to single-mode FoMs, wideband FoMs are inherently less intuitive, since they need to accommodate for more than one term and a balance between those terms must be found.

An effort was made to include the most relevant parameters into the new figure of merit. The FoM is not a dimensionless metric with a limit of 100%. A side effect of this is that a enormous spread of values is possible, since they don't need to be between one and zero. However, for the same reason it is therefore a great tool to compare two generators together since the values between them can be orders of magnitude instead of just a minuscule difference.

The parameter in FoM_{MM} which set it apart from other wideband FoMs, is the use of the integral of efficiency. The integral of efficiency is a measure of efficiency over the bandwidth, it seems comparable to using average power, but it uses efficiency information instead of power and efficiency peaks and power peaks do not necessarily overlap [7].

Future research

There is a substantial difference in the working principle of an array of resonaters and a generator where multiple modes are excited in a single body. In an array the multiple proof masses can vibrate independently due to their relative low mass compared to the mass of the vibration source. This means that the frequency of the vibration source can switch between resonance frequency of the first mode and the resonance peak of the second mode without disrupting the other proof masses. However, in a single proof mass multi-modal VEH this is not the case, switching between resonance frequencies means the entire mechanism must switch to the other frequency which itself takes time. If this frequency switching happens frequently, a substantial part of the energy yield may be lost in a single proof mass device as opposed to a multiple proof mass device. The extent to which this happens however is unclear and would be interesting to research.

2.6. Conclusions

Although vibration energy harvesters have been a research topic for two decades already, the practical implementation is still lacking. This is in part due to the fact that although VEHs have been getting more efficient on paper due to high quality factors and high resonance frequencies, this does not translate to high performance in real-world applications. For that reason, wideband VEHs have been getting more attention in research. In this paper a comprehensive overview of all available multi-modal VEHs based on compliant mechanisms is shown so that the reader has a clear idea of the available work done in this field and how it relates to each other. Also a new performance metric FoM_{MM} specifically developed to assess performance of wideband multi-modal VEHs has been introduced. This new metric is then used to assess the performance of multi-modal VEHs found in literature and it is shown that it does indeed favor generators with high bandwidth and high efficiency across the region of interest over those with a small bandwidth and/or low efficiency. In short, the new FoM_{MM} can be characterized by the following points:

- Multi-modal Vibration energy harvester overview
- FoM_{MM} Uses FoM_G as an overall efficiency metric to deduce how good the design of the generator is.
- FoM_{MM} Uses bandwidth information to include all resonance peaks.
- FoM_{MM} Includes integral of efficiency over region of interest to objectively gauge how much power output is possible in bandwidth.

Contributions

- Made a comprehensive overview of multi-modal vibration energy harvesters and mapped them in a clear way.
- Developed a new figure of merit able to assess multi-modal vibration energy harvesters performance.

3

On the efficiency of coupled vs uncoupled vibration energy harvesters under transient excitations

In this chapter, the main body of the thesis research is presented. It contains an introduction into the subject and research question of multi-modal vibration energy harvesting. The research methods are described followed up by the experimental results and corresponding discussion and conclusions. The references used in this paper are all grouped together with the references of the rest of the thesis, at the end of the thesis.

On the efficiency of coupled vs uncoupled vibration energy harvesters under transient excitations

M.W. Wouters, T.W.A. Blad and J.W. Spronck

Abstract

Vibration energy harvesters are especially interesting to use in an environment where there is one dominant vibration frequency present because then the harvesters can be designed to resonate at that specific frequency. To spread out the power yield over more frequencies a multi-modal harvester can be used which can resonate at multiple frequencies. A vibration with more than one sine wave can be manifested in a number of ways. The two frequencies can be present simultaneously, or they can alternate each other. How the energy harvesters react to these different vibration inputs is researched in this paper. Two fundamentally different multi-modal energy harvesters are used here. One which can be described by a coupled system of equations and one uncoupled. Two prototypes of an uncoupled and one coupled device are made and tested on an electromagnetic shaker. The vibration signals are sent to the shaker and the power output of the energy harvesters is measured using piezoelectric transducers mounted to the mechanisms. The results show that a phaseshift in the sine wave input signal generally results in a increase in power, where a decrease was assumed beforehand. When switching the input vibration from the first to the second eigenfrequency the power output does drop significantly, but the coupled mechanism has a substantially higher power output than the uncoupled device. And when the mechanisms are excited by a vibration with two eigenfrequencies at the same time no significant difference between the two can be observed, nor does the power output drop significantly. While the comparison between these two mechanisms is probably accurate, the quantitative conclusions must be taken with a grain of salt as it was noticed in a later stage of the research that the vibration signals were not consistent over the entire time period. At this point it is unclear if an overall better mechanism can be picked between the coupled and uncoupled one. However, it is shown that both have their distinct advantages where they outperform their counterpart, which can be used for designing a better energy harvester in future applications.

3.1. Introduction

Vibration energy harvesting is the act of scavenging energy present in ambient vibrations, and transducing that energy into other forms, electricity being the most common. These ambient vibrations can be observed in lots of different environments. Industrial processes like machinery operating at a certain frequency produce small amplitude, high frequency vibrations. Vibrations in the transport sector, like trains or trucks usually have a larger amplitude, but lower frequency vibrations [5]. Then there's the human body, whose vibrations can also be used for energy harvesting. This can be done in the form of human motion, for instance the walking motion where the impact of each footstep can be used. Or inside the human body, where heart contractions can be used to power an energy harvester. These stated examples all have wildly different values for amplitude, frequency and consistency. Generally speaking, a VEH is designed for the specific environment it is used for. They are most efficient at certain very specific conditions, and are very sensitive to changing conditions which usually means their efficiency lowers dramatically when their operation conditions are not met. This means that for every application the source vibrations must be thoroughly analyzed and a VEH design must be chosen which is best suited for that specific application. VEHs generally consist of three parts and can be approximated by a mass-spring-damper model. These three parts are: *Proof mass, suspension and transducer*

The proof mass is a mass which stores the kinetic energy of the vibrations. It is the mass in the mass-spring-damper model, so as it starts to move due to the ambient vibrations it builds up kinetic energy which will later be converted into electrical energy. The suspension provides the restoring force for the proof mass. VEHs are of a limited size, so the kinetic energy, which only requires motion is transformed into a vibration by means of a suspension which acts as a spring in the mass-spring-damper model. In small scale devices this is usually a flexure as coil springs are harder to manufacture in a small scale [26]. The third part of the VEH is the

transducer, which is the damper in the mass-spring-damper model. This part converts the energy from the kinetic to the electrical domain and also dampens the motion of the VEH. This can be achieved in a number of ways, which all have their use cases in different systems. The three most used principles are: Piezo-electric, electromagnetic and electrostatic. The model in this research uses a piezo-electric transducer which consists of a piezo foil connected to electrodes. As strain is put into the foil when the cantilever vibrates, a voltage is generated in the foil which can then be extracted using a rectifier and a battery.

Multi-modal vibration energy harvesting

For practical applications of vibration energy harvesting, multi-modal energy harvesters have a lot of potential because of their wideband power output. This means that the harvester is capable of generating significant power in a wider band of frequencies. A multi-modal generator is a VEH which has multiple distinct resonance modes. This is most commonly achieved by combining certain elements of the mass-spring-damper model in a way such that a coupled system of VEHs is created.

The VEH must be designed in a way such that power output is maximized. This means that the ambient vibrations must be analysed, and the resonance modes of the generator must match these ambient vibrations. However, even if the devices resonance modes are matched to the most prominent ambient vibration frequencies the output power can still be lower than can be expected if the device is slow to react to the constantly changing behaviour of the ambient vibrations. So the amount of times the source signal switches between prominent frequencies, or if frequencies are present at the same time can all influence the VEH power output.

A lot of research has already been done in varying forms of multi-modal vibration energy harvesting. Most of this research focuses on designing a wideband harvester, capable of significant power output over a wide range of frequencies. Su, Wu and Gong have designed in-plane cantilever harvesters using piezoelectric transducers [10],[28],[35]. Their research is based on maximising power output of their devices, but only looking at the steady-state frequency response. There are some less straight-forward and elaborate designs as well. Larkin [14] has designed a rotary hybrid harvester, and Leadenham [15] has used nonlinearity in a M-shaped harvester in an effort to increase power output. What most of this work has in common is that the mechanism characterisation is done using steady-state frequency response analysis, either experimentally or using a simulation.

This paper mostly focuses on finding out what entails good transient behaviour in VEHs, and what elements in a multi-modal VEH makes for good transient behaviour. This research can then be used to give recommendations such that in the future more efficient multi-modal VEHs can be designed for real world applications. In theory multi-modal VEHs have a clear benefit in that they can give a substantial power output over multiple frequencies, which would increase the power output in real world applications with multiple dominant frequencies. However there is a discrepancy between testing a VEH in a lab under controlled circumstances, and applying a VEH in an environment with real-world vibrations. The presumption is that this discrepancy can be partly explained by the fact that real-world vibrations with multiple dominant frequencies constantly change between these frequencies and VEHs are not putting out maximum power instantly when they are excited by a resonance frequency. It is instead assumed that a vibrating mechanism always takes a number of cycles to reach its full amplitude, which in the case of vibration energy harvesters means that transient phases in ambient vibrations cause a temporary drop in power output.The research objective is stated as follows:

In what manner do different types of multi-modal vibration energy harvesters react to transient behaviour in vibrations and to what extent does it reduce efficiency.

In the next section the methods used in this research are described, which contain the models and input vibrations used in this paper. The experimental setup is also shown in this section. After that the results of the experiments are shown in section 3. Following that is the discussion, where the results are analyzed and conclusions and recommendations for further research are shown.

3.2. Methods

As mentioned in the introduction, this research focuses on the difference between coupled and uncoupled multi-modal cantilever systems when excited with a vibration which has different types of transitions in it. To do this, first a model is made in Matlab. The model is made by deriving the equations of motion for both systems and by then deriving the relevant parameters for mass, stiffness and damping using commonly used equations. For the coupled system this means a set of two second order ODE's are composed. To solve this system using an ODE solver in Matlab the set needs to be rewritten to a set of four first order ODE's. So the set of second order equations which are also the equations of motion of the coupled system:

$$m_1\ddot{x}_1 = c_2(\dot{x}_2 - \dot{x}_1) + k_2(x_2 - x_1) + c_1(\dot{x}_0 - \dot{x}_1) + k_1(x_0 - x_1) \tag{3.1}$$

$$m_2\ddot{x}_2 = k_2(x_1 - x_2) + c_2(\dot{x}_1 - \dot{x}_2) \tag{3.2}$$

The masses m_1 and m_2 are comprised of both the mass of the proof mass, and the effective mass of the cantilever, which is equal to $\frac{33}{140}$ times the total mass of the cantilever [13]. The stiffnesses k_1 and k_2 are derived using linear beam theory and are checked using a precision force-deflection setup. The damping coefficients are only measured using the physical models and are derived using the logarithmic decrement method where the decay of the device is measured in free vibration, this method uses the amplitude of two consecutive peaks to determine the damping ratio ζ which can then be used to calculate the damping coefficient. In these equations x_0 represents the fixed world, which is also the driving force since no actual force is imposed but a displacement in the form of a vibration. These imposed input vibrations are stated in equation 3.5 to 3.7.

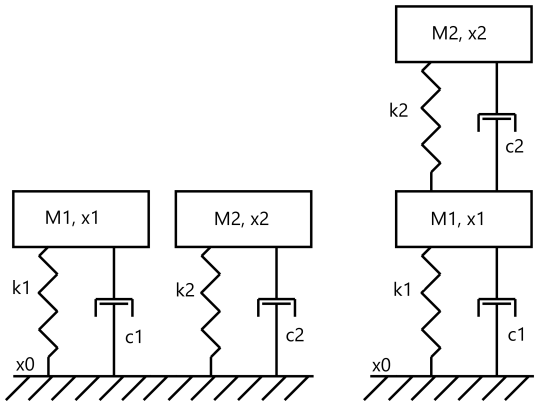

Figure 3.1: Schematic overview of the two prototypes used in this paper. The mechanism on the left hand side features two mass-spring-dampers fixed to the same world, hereafter called the uncoupled mechanism. The right hand side features two mass-spring-dampers stacked on top of each other, hereafter called the coupled mechanism. The input vibration is transmitted through the fixed world.

The uncoupled system of cantilevers is more straightforward to model since there is no interaction between both cantilevers, so it can be modeled using these two separate equations.

$$m_1\ddot{x} = c_1(\dot{x}_0 - \dot{x}_1) + k_1(x_0 - x_1) \tag{3.3}$$

$$m_2\ddot{x} = c_2(\dot{x}_0 - \dot{x}_1) + k_2(x_0 - x_1) \tag{3.4}$$

Using the system parameters stated in table 3.1 the resonance frequencies of both the coupled and uncoupled mechanism are located at around 16 and 22 Hertz. The resonance frequencies are matched deliberately so that the same input vibrations can be used for both of them. the mode shapes of both models are shown in figure 3.2 and 3.3.

(a) First mode, 16 Hertz (b) Second mode, 22 Hertz

Figure 3.2: First and second mode of the coupled mechanism. Mode analysis done in Comsol

(a) First mode, 16 Hertz (b) Second mode, 22 Hertz

Figure 3.3: First and second mode of the uncoupled mechanism. Mode analysis done in Comsol

The goal of research is to more accurately predict real-world performance, by testing the system behaviour under controlled conditions which mimic real-world vibration phenomena. In order to be able to make generalized conclusions using this research no real-world vibration signals are used, but some phenomenons one might find in practice are put into separate vibration signals. To guarantee the system is in steady-state prior to the disturbance in the signal the first 15 seconds of the signal are steady to let the system settle into its resonance mode. Then the disturbance takes place and then another 15 seconds so that the system can settle once again.

Experimental setup & measurements

To perform the measurements a setup is constructed. A schematic overview of this setup can be seen in figure 3.5. In this overview the laser sensor is shown, but the piezo foil transducer works in a similar manner. The setup essentially consists of two separate parts; a vibration output setup, and a vibration measurement setup. The vibration output is done using a vibration shaker which is controlled by a power amplifier and a NI DAQ device which holds a NI 9263 voltage output module, and a NI 9215 voltage input module for sensor

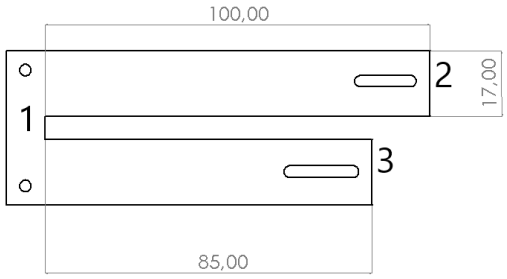

(a) **Dimensions of uncoupled mechanism. With the base at (1) and two proof masses at (2) and (3).**

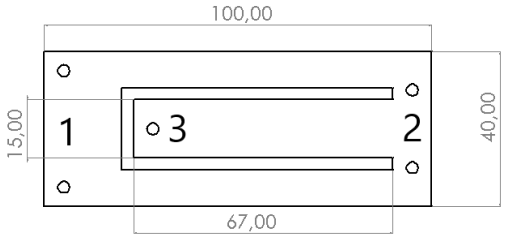

(b) **Dimensions of coupled mechanism. With the base at (1) and two proof masses at (2) and (3).**

Figure 3.4: **Dimensions of both models, 0.5 mm thick 301 stainless steel is used in both models.**

model specs	**m** [g]	**k** [N/mm]	**c** [-]
uncoupled			
long	1.62	112.5	0.0053
short	1.37	113.8	0.009
coupled			
outer	1.26	177.4	0.0257
inner	0.96	338.1	0.0618

Table 3.1: **Experimentally derived model specifications of both the coupled and uncoupled mechanism.**

measurement.

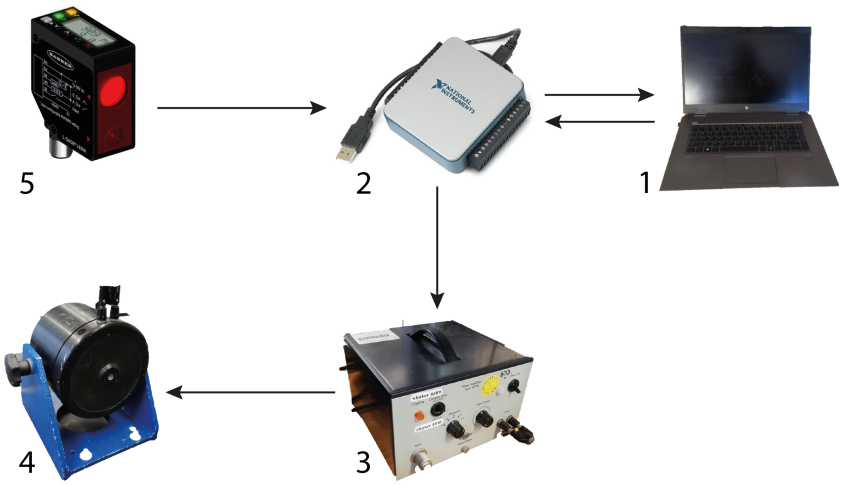

Figure 3.5: **Schematic overview of experimental setup. Where the computer (1) is connected to the data acquisition module (2), which has an input and an output module. The output module is connected to the power amplifier (3), whose output is fed to the shaker (4). The laser distance sensors (5) are connected to the input module of the DAQ (2), which is then fed back into the computer (1).**

The vibration measurement is done using two different methods. In first instance laser distance sensors were used, pointed at the ends of the cantilevers. since all resonances of the mechanisms are first order, the endpoint deflections are representative for overall strain in the cantilever elements. In all measurements, both endpoint deflections were measured, as well as base vibration. Since the shaker has limited power and stiffness, there is certain distortion between the output signal and the actual vibration profile transmitted by the shaker. Also, the base connecting the shaker to the mechanisms has limited stiffness so there is an overall transfer function between the designed vibration signal and the vibration that is fed into the mechanism. In figure 3.7a and 3.7b the output signal, and measured signal at the base of the VEH mount is compared. In figure 3.7a the uncoupled VEH is mounted, so it shows how the shaker can still put out the required signal with acceptable sharpness with the full weight of mount and mechanism attached.

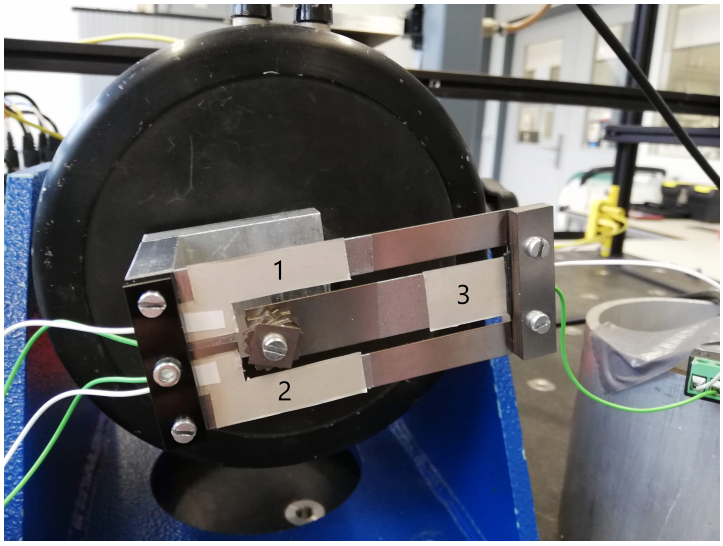

Figure 3.6: **Coupled mechanism mounted on shaker. The parts indicated by (1),(2) and (3) on the cantilevers are the piezofoil transducers. Each piezo foil element has two insulated copper wires running to the NI DAQ module. One of these wires is connected to the bottom electrode attached to the cantilever. And the other one is clamped on top of the piezo foil, the top electrode.**

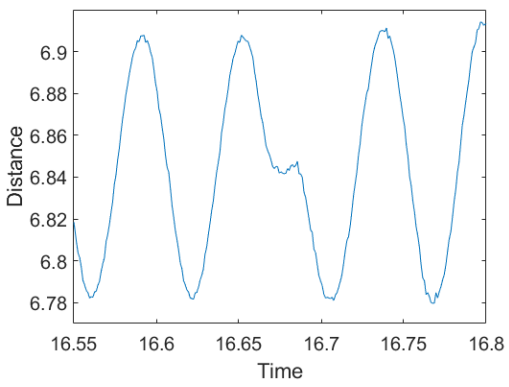

(a) **Output signal of 120°phaseshift.**

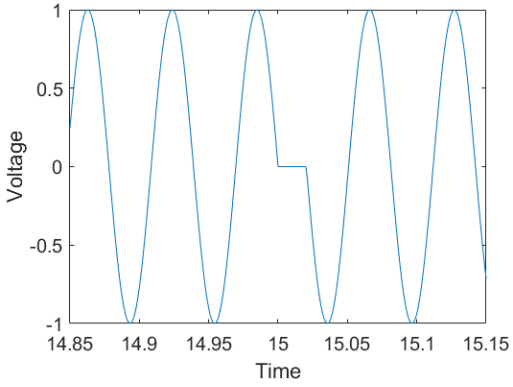

(b) **120°phaseshift measured at base.**

Figure 3.7

Measurement procedure

The vibration signals used in the measurements are the following, they are also visualized in figure 3.8a to 3.8c:

$$y(t) = Y_1 sin(\omega_1 t) + Y_2 sin(\omega_2 t) \tag{3.5}$$

$$y(t) = \begin{cases} Y_1 sin(\omega_1 t) & \text{for } 0 < t \leq \frac{1}{2} t_t \\ Y_2 sin(\omega_2 t) & \text{for } \frac{1}{2} t_t \leq t < t_t \end{cases} \tag{3.6}$$

$$y(t) = \begin{cases} Y_1 sin(\omega_1 t) & \text{for } 0 < t \leq \frac{1}{2} t_t \\ 0 & \text{for } \frac{1}{2} t_t < t \leq \frac{1}{2} t_t + \beta \\ Y_1 sin(\omega_1 t + \beta) & \text{for } \frac{1}{2} t_t + \beta \leq t < t_t \end{cases} \tag{3.7}$$

In equation 3.5 two separate sine signals are added together with two different amplitudes and frequencies.

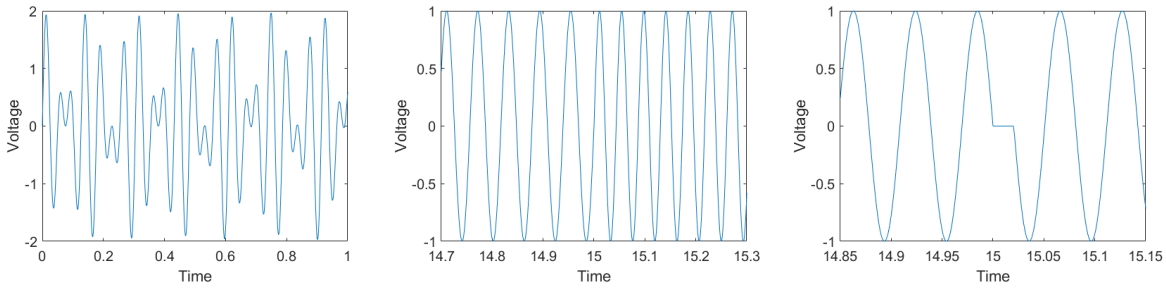

(a) **Simultaneous sine** (b) **Alternating sine** (c) **120°phaseshift in sine signal**

Figure 3.8: **The vibration signals sent out to the shaker**

In equation 3.6 two signals with different amplitude and frequency are alternated, so first only the first signal is present which then changes into the other one with different frequency. In equation 3.7 the signal starts with a normal sine wave, then at $t = \frac{1}{2}t_t$ a phaseshift is introduced. In practice this means that the signal is zero, until the desired phaseshift has been achieved and then the same sine wave is excited again. In the phaseshift signal, β varies between 30 and 180 degrees, which represents the degrees of phaseshift achieved.

A mechanism with finite, non-zero mass and stiffness always has a certain transfer function between input and output vibrations. If the mechanism has multiple modes and if these modes are coupled, there can be a substantial difference between the different vibration inputs portrayed in figures 3.8a to 3.8c. The reason why looking at the dynamic behaviour of these mechanisms excited by transient vibrations is interesting is because it has a big influence on power output in real-world applications. It is also assumed there is a substantial difference in transient behaviour between VEHs with different layouts as shown in figure 3.4.

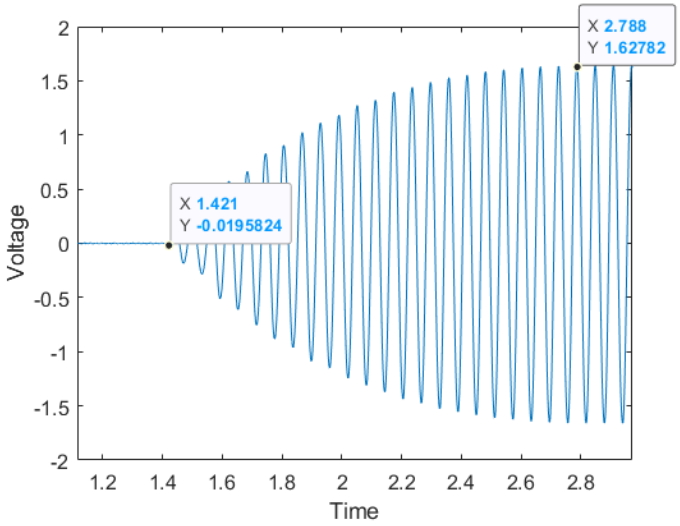

Figure 3.9: **Ramp-up time of outer cantilever of coupled mechanism. t_1 = 1.4 indicates the start time where the shaker starts vibrating. t_2 = 2.8 indicates the point where the cantilever has reached its maximum amplitude.**

In all the vibration signals used in this research t_t is 30 seconds, which means that the system has 15 seconds to reach a steady-state vibration from its rest position, and then the input signal changes at $\frac{1}{2}t_t$ as described in equation 3.5 to 3.7. After the change at $t = 15s$ the system has another 15 seconds to reach steady-state before the input vibration is terminated. As can be seen in figure 3.9, the coupled mechanism takes about 1.4 seconds to reach a steady-state vibration mode from a rest position, which equals to roughly 22 vibrations using a 16 Hertz vibration input. However, this period can be considerably longer if the input vibration is actively counteracting the free vibration of the mechanism.

3.3. Results

As stated in the previous section the vibration measurement was done using two different techniques; using laser distance sensors, and using piezo foil as a transducer on the mechanism itself. The results are reported using the data generated from using the piezo foil as that is also the premier choice for practical applications. By using the piezo foil we also include any dynamic effects the added mass and stiffness may have on the mechanism. Also, especially in the coupled mechanism the translation between end point deflection and cantilever strain is not entirely trivial. Other than end point deflection also end point rotation must be taken into account since the two cantilevers are coupled. Only using end point deflection measurement, rotation is impossible to gauge so using piezo foil is the most straightforward and inclusive solution.

Since the long cantilever is in resonance in the chosen phaseshift signal, that is the one which has the slowest transient since it has more kinetic energy built up in the leafsprings.

Also for the sake of improving power output, it makes sense to focus on the resonance mode, since the power output of the cantilever in resonance is roughly 20 times higher than the non-resonance cantilever. This can be seen in figure 3.10a and 3.10b. So here we look primarily to the long cantilever, but also a comparison between the different behaviour of the short cantilever will be observed.

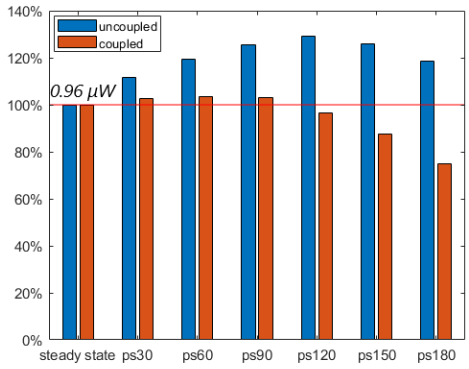

(a) **Power output of first mode of coupled and uncoupled mechanism under phaseshift excitation, compared to steady-state output of both devices.**

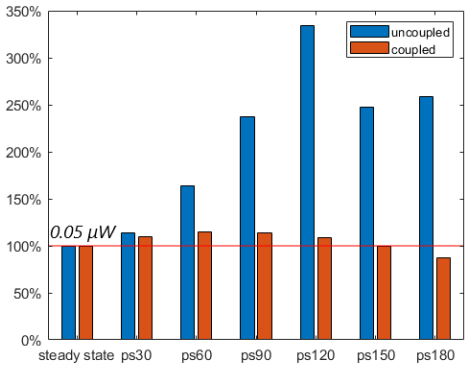

(b) **Power output of second mode of coupled and uncoupled mechanism under phaseshift excitation.**

Figure 3.10

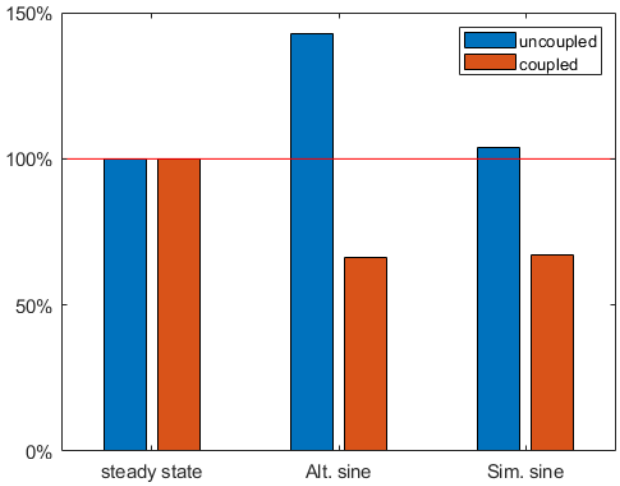

Figure 3.11: **Combined power output of both modes of coupled and uncoupled device under alternating and simultaneous sine excitation.**

Figure 3.10a and 3.10b contain the power output figures of both the coupled and uncoupled mechanism for all phaseshift vibration signals as described in the methods section. Figure 3.11 shows the power output figures of both mechanisms for the simultaneous and alternating input vibration signal combined. The first set of bars in all result figures correspond to the steady-state power output of both mechanisms and is 100% by definition. This means that the output of the device when excited by all the different phaseshift input signals is compared to this steady-state power output value. The phaseshift result figure 3.10a applies to the first mode at 16 Hz and the figure on the right 3.10b applies to the second mode, at 22 Hz. As can be seen in figure 3.2 to 3.3 this means that the figures on the left hand side apply to the outer cantilevers in the coupled mechanism, and the long cantilever in the uncoupled mechanism.

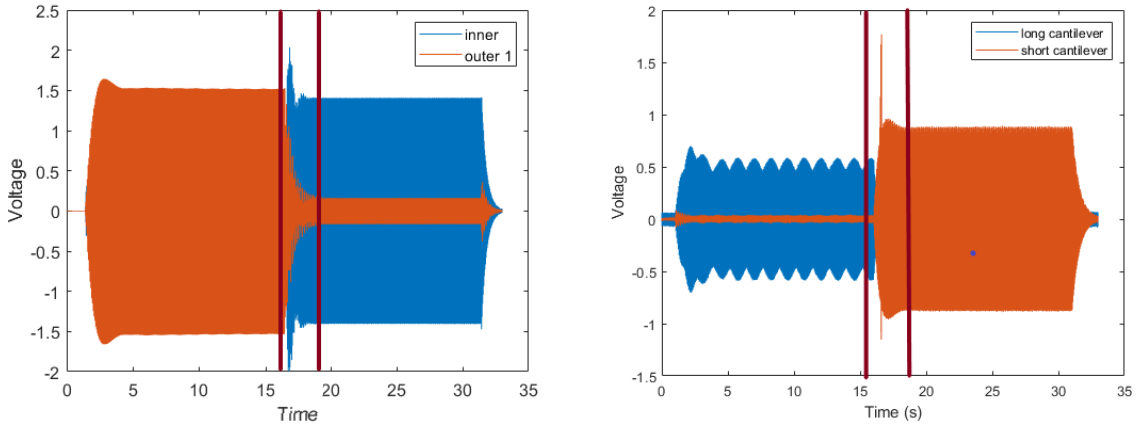

(a) **Coupled mechanism, alternating sine input.**

(b) **Uncoupled mechanism, alternating sine input.**

Figure 3.12

Figure 3.12a and 3.12b compare the responses of the coupled mechanism and the uncoupled mechanism under an alternating sine excitation. The red lines indicate the region which is considered the transient region, where the power output is disturbed due to the switch in frequency in the input vibration and it is reaching a steady-state again. In figure 3.12b we see a certain wave-like phenomena in the response of the uncoupled system. The power output does not reach a steady-state value but keeps bouncing around between an upper and lower limit. The same can not be observed in figure 3.12a.

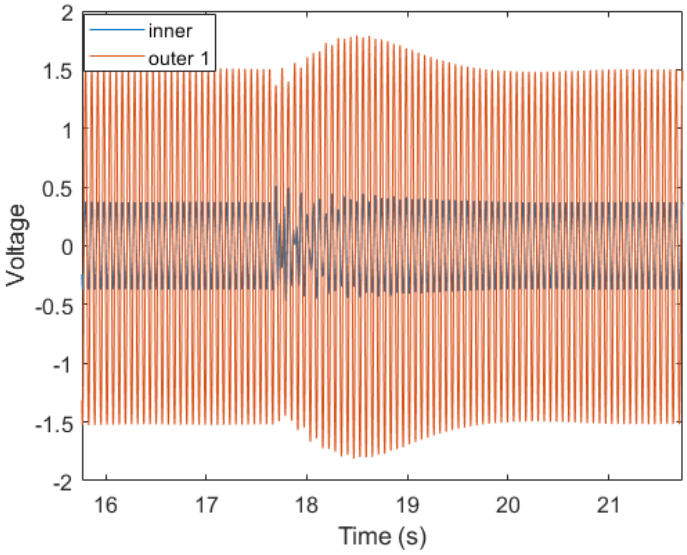

Figure 3.13: **Timeseries plot of the coupled mechanism with a 90°phaseshift excitation at around 17.8 seconds. The orange lines indicate the outer cantilever which is in resonance mode. As we can see the output voltage of the outer cantilever almost immediately goes up after the phaseshift phenomena.**

3.4. Discussion

To gauge how well the mechanisms react to the different phaseshift vibration inputs, we look primarily to the resonance mode since the power output is around 20 times higher than the non resonance mode in both mechanisms. So even though the power output increase or decrease might be higher percentage wise in the non resonance mode, when looking at pure power difference it falls behind when compared to the resonance mode. The hypothesis stated earlier in this paper said that a drop in power was expected when basically any sort of transient phenomenon is introduced in the vibration signal. This makes sense, because a cantilever has its highest amplitude at its natural frequency. And due to the relatively high quality factor of these designs, reaching the maximum amplitude can take a considerable amount of vibration periods. So disturbing the steady-state vibration would logically temporarily lower the power output, which would then take a reasonable number of vibration periods to reach its previous maximum amplitude state again. For that reason some of the results stated in the previous section come as a surprise. Especially in the graph showing the various degrees of phaseshift we can see an overall increase of power output, only falling below 100% of steady state output when the phaseshift reaches 120° and up. When looking at the timeseries in figure 3.13, we can see that at the exact time the phaseshift is excited on the shaker, the power output goes down very momentarily before it comes up again and reaches a level higher than the steady-state value. This temporary higher state of power output lasts for a longer time than the lower state power output right after the phaseshift, so overall the the power output over the entire transient period is higher than the average steady-state power output. Unfortunately this seems to be due to a mistake made in the vibration signal instead of a real repeatable phenomenon. More on this in the next subsection *What went wrong*.

The results show that the uncoupled mechanism reacts better to the phaseshift input as its power output is higher than the corresponding coupled mechanism power output in all phaseshift variations. This is true for both the first and second mode. This is somewhat expected since there is no interference between the two cantilevers in the uncoupled mechanism. Which means that, for equal total dimensions, there is less kinetic energy stored in the long cantilever of the uncoupled mechanism as compared to the first mode of the coupled mechanism where the entire mechanism is in resonance because the mode shape consists of both the inner and outer cantilevers as can be seen in figure 3.2a. This also means that more kinetic energy needs to be 'disturbed' in the coupled mechanism as compared to the uncoupled mechanism. The same phenomenon can be observed in the remaining two vibration inputs. the uncoupled mechanism outperforms the coupled mechanism in both the alternating sine and simultaneous sine vibration. Again, the uncoupled mechanism is performing better than the steady-state value during these transient periods. The expectation is that this is due to the same phenomena described in subsection *What went wrong*.

What went wrong

The main outcome of this research is the comparison between an uncoupled versus a coupled mechanism when excited by several special input vibrations. A very unexpected outcome of this experimental study is the increase in output power of both mechanisms when a phaseshift is transmitted through the shaker. Logically, this makes no sense as effectively the shaker is disrupting the resonance mode of the mechanisms, which should lower its power output as the resonance mode is the highest possible power output imaginable. The main culprit proved to be the vibration signal itself. After a transition phenomenon, like a phaseshift or a switch in frequency, the signal amplitude proved to vary quite significantly. This variation in vibration amplitude, caused the amplitude of the cantilevers of the mechanism to spike in amplitude, which increased the power output. The fact that the base and mechanism themselves have significant mass as compared to the shaker, caused one of the main assumptions when comparing reality to experimental setup to not be satisfied. Namely that the dynamics of the VEH mechanism do not influence the dynamics of the shaker. Such an assumption can only be made when the mass of the VEH mechanism is negligible compared to the shaker, or when the shaker is actively controlled. Both of which do not apply in this case. So because the amplitude of the shaker vibration is not controlled, but instead only the output voltage is regulated without feedback, there is a substantial variance in shaker vibration amplitude when the mounted mechanism exerts a force on the shaker. This effect can be seen in figure 3.14. The arrow in figure 3.14 indicates the moment the phaseshift is excited. Afterwards, the amplitude of the base vibration immediately goes up by around 25% before it eventually settles down again at the pre-phaseshift amplitude. However, that takes a coupled

of seconds, which means that the uncontrolled shaker is an inadequate source of vibration signal and is also influencing the dynamics of the mechanism in the meantime.

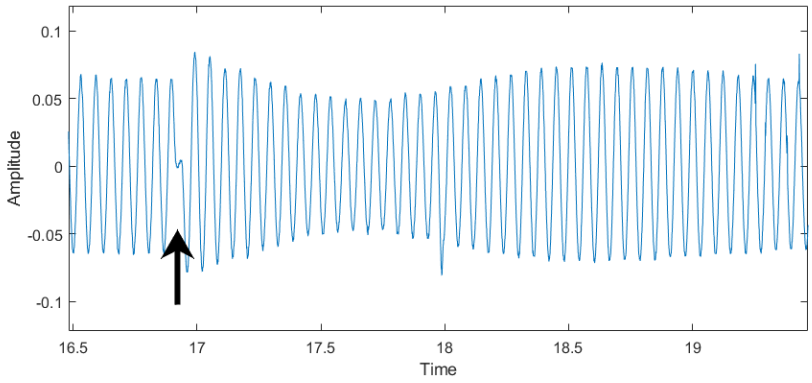

Figure 3.14: **Movement of base with 180°phaseshift vibration input with the uncoupled mechanism mounted. The phaseshift can be seen at around 17 seconds, and subsequently the amplitude of the vibration is changing as a result of the disruption of the effective mass of the mechanism.**

Further research

The goal of this research was to show that real-world performance might differ from standard lab test performance when only sine sweeps or constant sine waves are used. An effort is made to replicate real-world vibrations by using some specific phenomena one might find in practice. However, as stated before it turned out that the vibration signal used were not of sufficiently high quality that any meaningful conclusions about the in- or decrease of power output can be made. A logical follow up on this research would then be to add active control to the vibration setup so that the vibration signal remains constant, not influenced by the dynamics of the harvester mechanism.

Also, it remains unclear how these systems would react to vibrations which are a combination of the signals we used in this research or if the signals themselves are not clean sine waves but slightly asymmetric or another special form. Another follow up on this research would thus be to continue to research these devices on real-world vibration signals to see if there is any considerable difference between the results found here in this research and real-world vibrations.

Conclusions

In this work we have found differences in the power output of coupled versus uncoupled mechanisms when excited by between coupled and uncoupled mechanisms in vibration energy harvesting. The uncoupled mechanism outperforms the coupled mechanism in all tested situations. At 30°phaseshift the power output difference is 9% and it continually grows up to 58% when the phaseshift is 180°. This seems to be due to the fact that in the coupled mechanism both cantilevers are a part of both modeshapes. To change these modeshapes means changing the ratios in which these cantilevers participate in the modeshape which understandably takes longer than for a separate cantilever to change to a bigger amplitude. Furthermore, the performance difference becomes more pronounced as the amount of phaseshift becomes larger.

When excited with two simultaneous sine waves, the uncoupled device outperforms the coupled device by 55%. The uncoupled device in the transient region even outperforms its steady-state value slightly, by 4%. However, that value is inflated due to a non-constant excitation amplitude. When excited by an alternating sine wave, the uncoupled device outperforms the coupled device by 115%. In our test the power output of the uncoupled device was 142.9% of the steady-state value, compared to 66.2% of the coupled device. Again, the absolute values should be taken with a grain of salt but the comparison between the two does hold.

Generally speaking we can not make any certain statements regarding the validity of these conclusions. The

claim that the power output of these devices rises when excited by a disturbance, is doubtful and most likely due to the lack of active control on the vibration signal. The between device comparison is more likely to be correct, but a follow-up on this should be done to make any definitive conclusions.

4

Reflections, conclusions and recommendations

This chapter reflects on the entire graduation project, including literature study and thesis research. The research activities are presented, both the successful ones which made it into this thesis and the unsuccessful ones which were abandoned due to various reasons explained in this chapter. Some general conclusions and recommendations for future research are also presented here.

4.1. Research activities

Over the course of this project a number of different research activities were undertaken. The following overview is shown to give the reader a clearer view of the order of which the different activities follow up on each other, if the thesis itself has not done so.

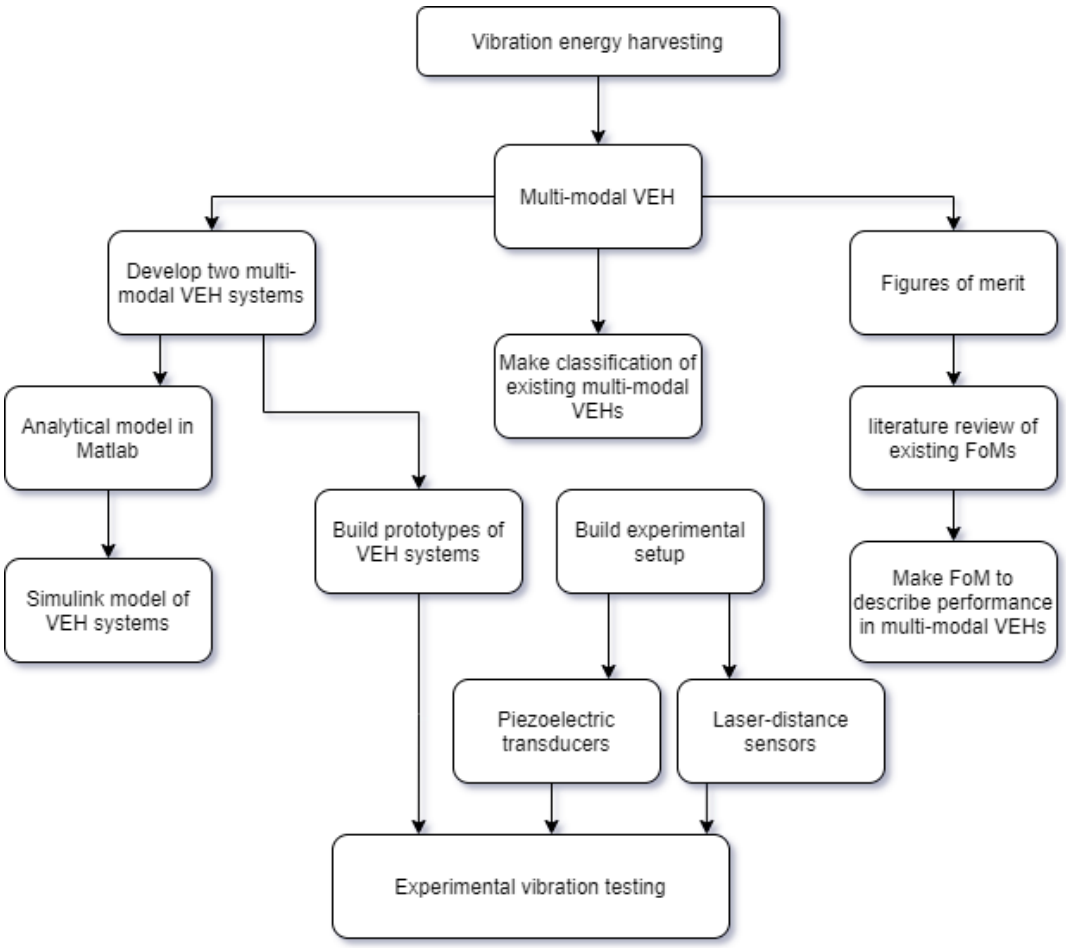

Figure 4.1: **Overview of research activities over the full course of the thesis project.**

4.2. Conclusions

Here some conclusions are shown regarding the project itself, not so much about the work done in the project as those are stated in chapter 3. The statements here can be seen as more personal conclusions and takeaways from the author.

The main takeaway, which has costed a lot of time in this project, is to always keep a short line between theoretical modeling and verifying that theoretical work. The verification can be either done by another analytical method, or by experimental validation. Because the time frame between doing the Simulink analysis and the experimental validation in the lab was so long, most of the time spend composing and writing simulation results was discarded because in the end it proved to be very unreliable. Of course Covid-19 was the main reason a direct experimental validation was difficult to achieve, but other methods could have been explored.

Another important learning point was that it is very easy to spend too much time dwelling on choices made, when it is clear in an early stage a bit of backtracking is needed to continue in a new line of research. For example the experimental setup initially only included laser-distance sensors, when it was very clear more

information was needed to be able to make conclusions about the dynamic behaviour of the systems. Still, it took a considerable amount of time before the piezo-electric transducer possibility was seriously considered.

In the same line a lot of time was spend writing detailed elaborate pieces of text only for it to be scrapped because the scope of the project changed considerably, or the results proved to be faulty. In future projects the preliminary results will be written down briefly, and then expanded upon when the scope and direction of the project is fully set.

Finally a list of practical recommendations for future work.

- At (almost) every step of the experimental validation process the consequences of a choice you make should be clear. Make basic steps for which it is still possible to track down the consequence.
- At high-frequency vibration, absolute stiffness does not exist. Make sure the parts which should be 'stiff' are adequately so.
- When sourcing equipment, think ahead and contact external people/resources as early as possible to avoid unnecessary delays.
- When trying to eliminate noise from your experimental data, sometimes it is not most effective to try to think rationally. In the end grounding every piece of equipment separately has worked. At this point it is still unclear where the excessive levels of noise in the signal originated from.

Acknowledgements

First and foremost I would like to thank my direct supervisors, Thijs Blad and Jo Spronck for the opportunity to embark on this project under their guidance. They have been an invaluable resource of knowledge and guidance and really helped shape this project into its final form. Although they left the responsibility of managing the responsibility completely to me, I could always count on their input and critical feedback.

Next I would like to show my gratitude to the rest of the energy harvesting group of the department. In these strange Covid times they have been a much needed source of companionship, without which this process would have been much more solitary while we were all working from home. Of course next to the companionship the critical input during the weekly meetings and help offered with trouble shooting experimental setups and lab equipment is just as valuable. Thanks to my housemate and friend, Dennis and Mathijs for their levelheadedness and their ability to put things in perspective and in that way contributed to the completion of this thesis and my sanity. Their perspective, tips and words of advice definitely helped shape this thesis for the better.

I would like to thank my parents for their support during this time, and for all the years leading up to this moment. Without their support and approval I would not be where I am today.

The greatest supporter throughout this entire period has been my partner, Steffie Ballemans. She filled the role of emotional support, motivator and sparring partner. Without her support this project would have been a whole lot harder and her part cannot be understated.

A

Model generation

In order to make a coupled and an uncoupled system with the same dynamic characteristics the resonance frequencies of the coupled mechanism must match the one of the uncoupled mechanism. In this Appendix the general equation of motion for a mass-spring-damper system is introduced, and then the system matrices of the different models are used to solve the equations of motion.

The general form of the equation of motion for a mass-spring-damper system can be derived by examining the sum of forces on the system. The assumption in these equation is that the system can be approximated by a lumped mass model, which means the mass of the spring and damper are negligible compared to the total mass of the system.

$$\sum F = -kx - c\dot{x} + F_{external} = m\ddot{x} \tag{A.1}$$

Where F are the forces acting on the system, k is the stiffness of the spring, c is the damping and m is the mass. This standard equation can be rearranged and some ratios can be introduced which lead to the following equation:

$$\ddot{x} = 2\zeta\omega_n\dot{x} + \omega_n^2 x = u \tag{A.2}$$

Where $\omega_n = \sqrt{\frac{k}{m}}$; $\zeta = \frac{c}{2m\omega_n}$ and $u = \frac{F_{external}}{m}$. Here ω_n is the natural frequency and ζ is the damping ratio.

Equation A.1 and A.2 are valid for one degree of freedom mass-spring-damper systems but can easily be extended to include multiple degree of freedom systems by replacing the scalars; k, c and m for matrices. The square matrices are then the same dimension as the number of degrees of freedom present in the system.

Effective mass & Effective stiffness

For the analytical model the lumped mass model is used to represent the two different VEH systems. However, the mass of the cantilever beam is in the same order of magnitude as the mass of the proof mass so it is not negligible in this model. For that reason the effective mass of the mechanism including the cantilever beam must be calculated. A mass of $\frac{33}{140}$ [13] times the total mass of the cantilever can be added to the proof mass to account for the distributed mass of the cantilever itself.

Using this value for mass of the cantilever and using the values for stiffness and damping as measured on the real mechanism yields a

Uncoupled mechanism

Placing the resonance frequencies of the uncoupled mechanism at the positions we are interested is relatively straightforward. The mechanism is assumed to be approximated by a lumped mass model. So that means the mass of the flexures themselves are small with relation to the masses of the proof masses as can be seen in chapter 3. If the lumped mass model assumption is correct the resonance frequencies of the uncoupled model can be approximated by linear beam theory. Linear beam theory holds if the displacements are relatively small and the cantilevers themselves act as linear springs, which is true if they are slender enough. equation A.3 gives the natural frequency of a mass spring system with stiffness k and mass m.

$$f_n = \frac{1}{2\pi}\sqrt{\frac{k}{m}} \tag{A.3}$$

Where in the instance of a cantilever beam the stiffness is governed by equation A.4.

$$k = \frac{3EI}{L^3} \tag{A.4}$$

This means that if we are making a mechanism with two uncoupled cantilevers out of the same sheet of metal, the only two parameters we can vary are the mass at the end of the cantilever and the length of the beam.

In practical applications volume or mass restrictions may be of concern so then it is convenient that both those parameters can be varied to reach the same goal. In our case the goal is to make a device with two distinct resonance frequencies and to improve the dynamic performance of the experimental setup the weight is reduced to a certain degree. For that reason a mechanism with a long and a short cantilever is designed as can be seen in figure A.1. According to equation A.4 the stiffness is proportional to the length cubed. So an increase in length of 17% accounts for a decrease in stiffness of 60%. Since the resonance frequency is a function of the square root off the stiffness the resonance frequency shift from increasing the length by 17% is 26%. These relations have been used to design an uncoupled cantilever mechanism with two resonance frequencies located at 16 Hz and 22 Hz.

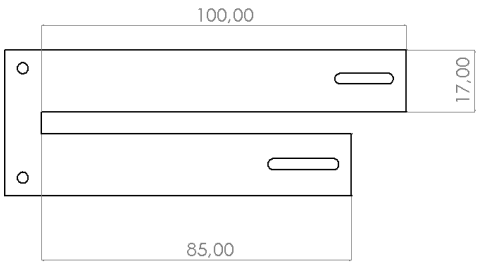

Figure A.1: **Drawing of uncoupled mechanism.**

Coupled mechanism

The design of the coupled mechanism is a bit more involved since the two cantilevers affect each other when vibrating so the equations governing the resonance frequencies are coupled. The theory behind these equations is found in [36]. They used a method where the stiffness and mass matrices are composed using parametric elements. And then those parametric matrices are used to derive an expression for the resonance frequencies.

$$[M] = \begin{bmatrix} M1 & 0 \\ 0 & M2 \end{bmatrix} = M1 \begin{bmatrix} 1 & 0 \\ 0 & \alpha \end{bmatrix} \tag{A.5}$$

The stiffness matrix of the coupled mechanism is also derived by Wu et al.

$$[K] = \frac{6EI}{(3\beta^2 + 4\beta^3)L_1^3} \begin{bmatrix} 2 - 6\beta + 6\beta^2 + 2\beta^3 & 3\beta - 2 \\ 3\beta - 2 & 2 \end{bmatrix} \tag{A.6}$$

Here, the symbol α denotes the proof mass ratio of the mechanism M2/M1. And β denotes the ratio of the effective length of the cantilevers in the mechanism, L2/L1.

Then the massmatrix and stiffnessmatrix can be used to solve the eigenvalue problem to obtain the two resonance frequencies.

$$\frac{\Delta(\omega^2)_{1,2}}{\omega_s^2} = \frac{4\sqrt{[\alpha(1 \pm 3\beta + 3\beta^2 + \beta^3) + 1]^2 - \alpha(3\beta^2 + 4\beta^2)}}{\alpha(3\beta^2 + 4\beta^3)} \tag{A.7}$$

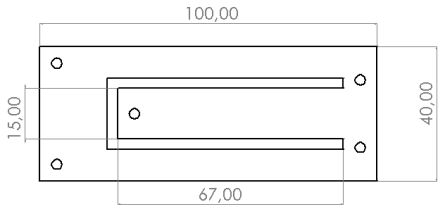

Figure A.2: **Drawing of coupled mechanism.**

System matrices

The system characteristics of the physical model were measured as accurately as possible so that the Matlab model can be build according to the real world specifications. In this way, any differences between the physcial properties derived from theoretical equations and the physical model will be eliminated. differences

between real stiffness and theoretical stiffness based on linear beam theory can occur because of linearization effects when the amplitude of the deformation gets relatively high. Also there are slight differences in stiffness based on geometry which linear beam theory can not account for. For instance the slots made at the end of the cantilevers made for slight alterations of the location of the proof masses detract a bit of stiffness from the overall cantilever.

Uncoupled system

for the uncoupled system the system matrices are relatively straightforward since there is no coupling between the two separate cantilevers.

$$K = \begin{bmatrix} K1 & 0 \\ 0 & K2 \end{bmatrix}$$

$$M = \begin{bmatrix} M1 & 0 \\ 0 & M2 \end{bmatrix}$$

B

Setup specifications

The practical equipment conducted in this research are done in a controlled lab environment using the equipment and protocols listed below.

- Connect NI DAQ device to laptop1 using USB cable.
- Plug in NI DAQ device to power.
- Turn on amplifier and keyence laser sensors.
- Mount VEH mechanism on shaker using M8 bolt.
- Boot Matlab and Matlab analog input recorder.
- Select relevant channels in analog input recorder to log laser sensor output.
- Start Matlab script to output vibration signal to shaker.
- Start analog input recorder recording.
- Save keyence laser sensor data.

Equipment	**Specification**	**Unit**
Shaker B & K type 4809	Frequency range	10-20.000 Hz
	Max acceleration	75 g
	Max displacement	8 mm
NI DAQ	Measurement resolution	16 bit
	Impedance	200 kOhm
	Sample rate	100 $kS/s/ch$
	Measurement range	$\pm$ 10 V
Keyence laser sensor	Sampling rate	opzoeken
	Measurement range	$\pm$ 10 mm
	Spot diameter	25 μ
NI simultaneous analog input 9215	Voltage range	-10 V to 10 V
	Number of bits	16 Bits
	Max sampling rate	100 Ks/s
NI output module 9263	Voltage range	-10 V to 10 V
	Number of bits	16 Bits
	Max sampling rate	100 Ks/s
	Max current drive	1 mA
Piezo sheet TE connectivity	Thickness	110 μm
	Mechano-electrical conversion	400 $\frac{mV}{\mu m}$

C

Results

Some results in its raw format are shown here to give the reader an idea of how the different mechanisms react to the vibration inputs. The images on the left hand side feature the full length experiment data, where the blue and orange colors indicate the location data of the two different cantilevers of the two models. The two dark red vertical lines indicate which part of the timeseries is used for the power output analysis, which is indicated in the figures on the right hand side. The figures on the right hand side feature the same data but are zoomed in.

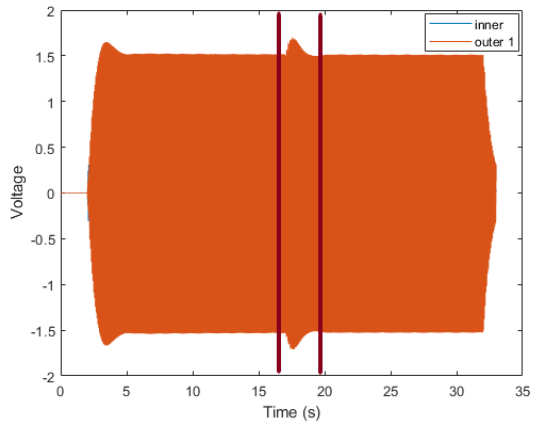

(a) **Coupled mechanism, phaseshift 30°**

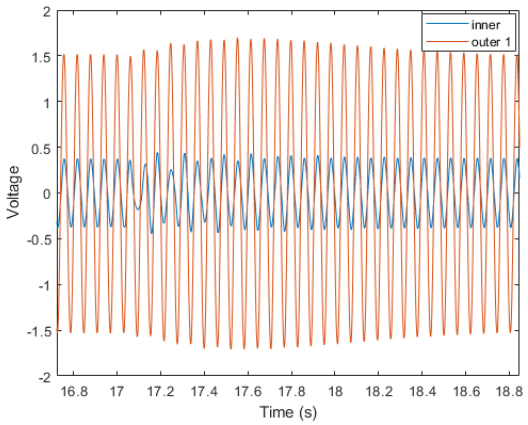

(b) **Transient dynamic behaviour section of graph (a).**

Figure C.1

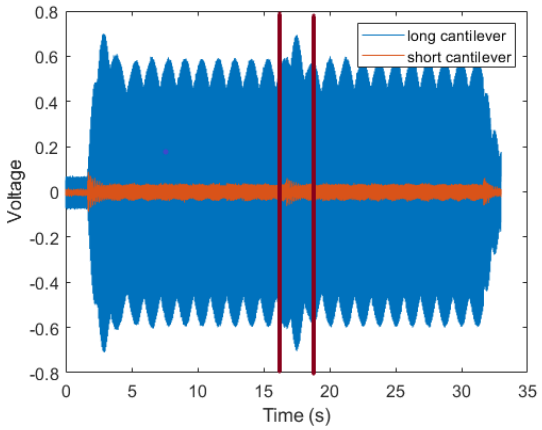

(a) **Uncoupled mechanism, phaseshift 30°**

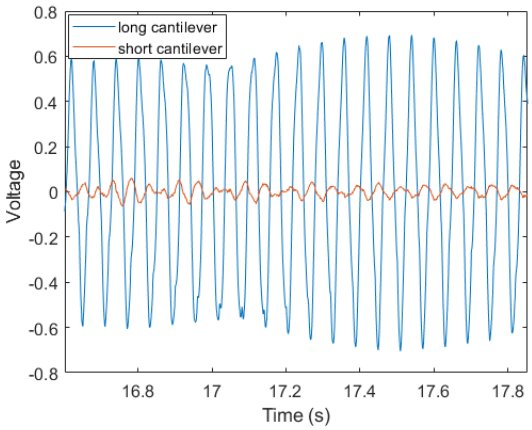

(b) **Transient dynamic behaviour section of graph (a).**

Figure C.2

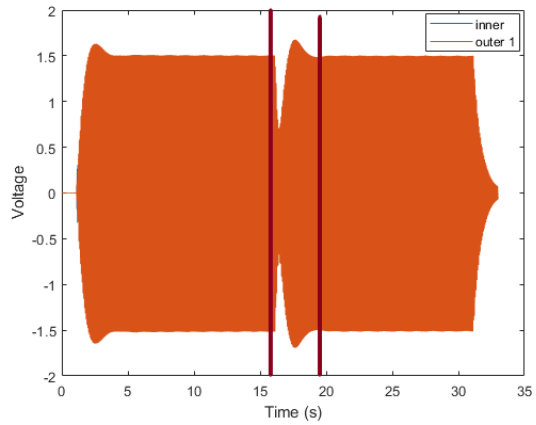

(a) **Coupled mechanism, phaseshift 180°**

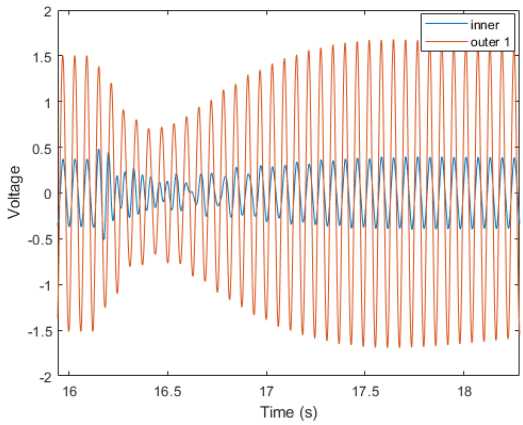

(b) **Transient dynamic behaviour section of graph (a).**

Figure C.3

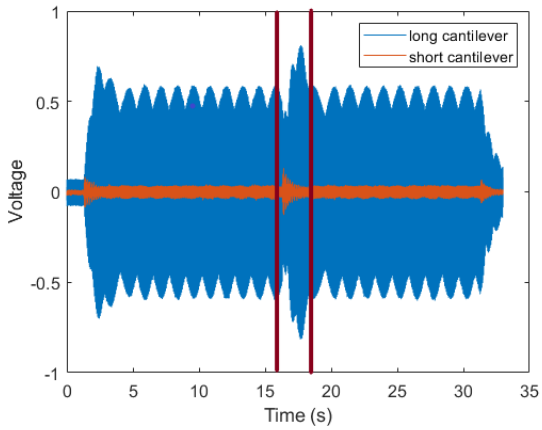

(a) **Uncoupled mechanism, phaseshift 180°**

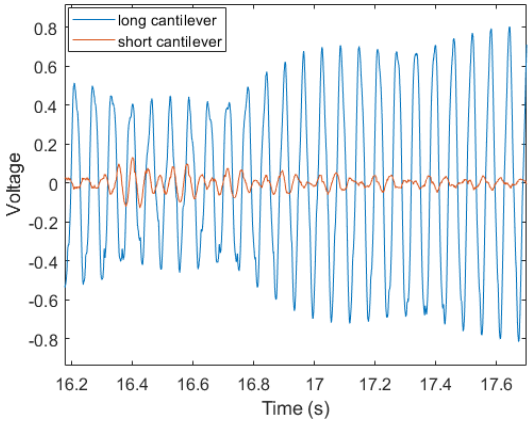

(b) **Transient dynamic behaviour section of graph (a).**

Figure C.4

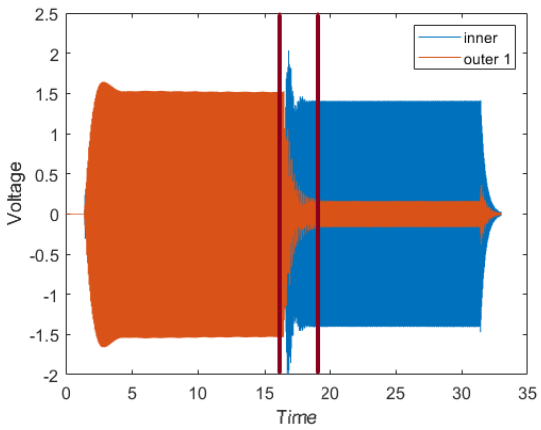

(a) **Coupled mechanism, alternating sine input**

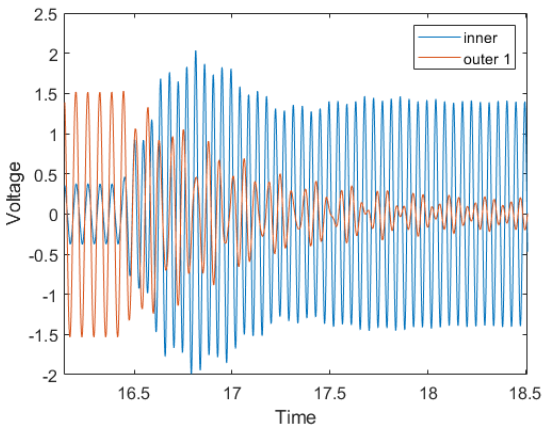

(b) **Transient dynamic behaviour section of graph (a).**

Figure C.5

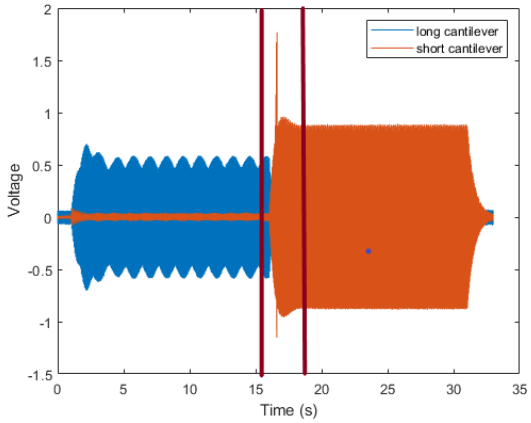

(a) **Uncoupled mechanism, alternating sine input**

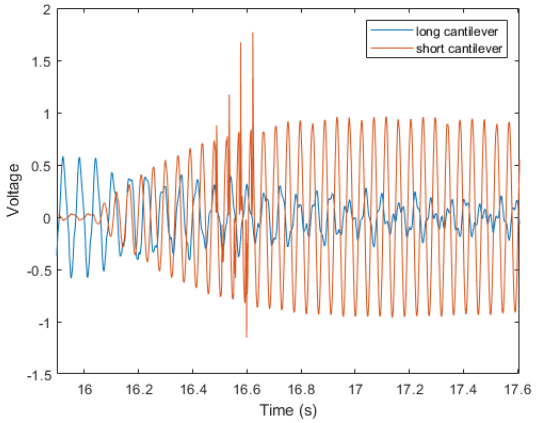

(b) **Transient dynamic behaviour section of graph (a).**

Figure C.6

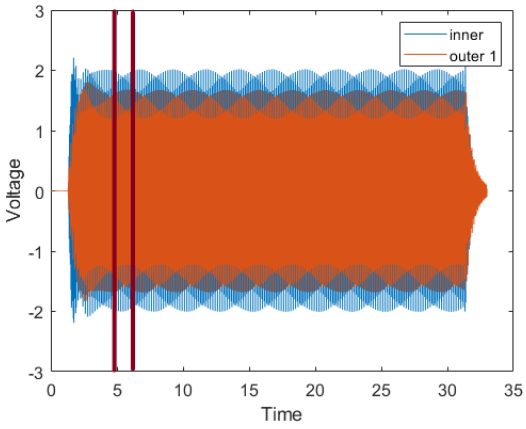

(a) **Coupled mechanism, simultaneous sine**

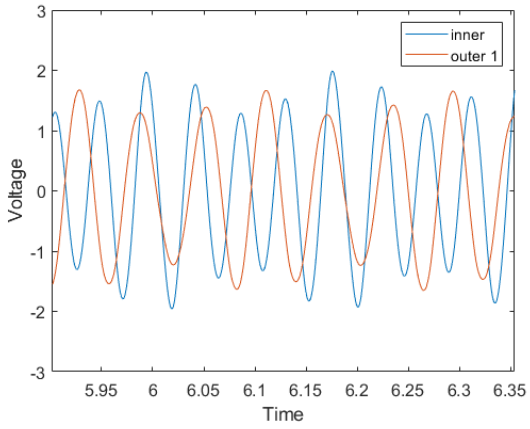

(b) **Transient dynamic behaviour section of graph (a).**

Figure C.7

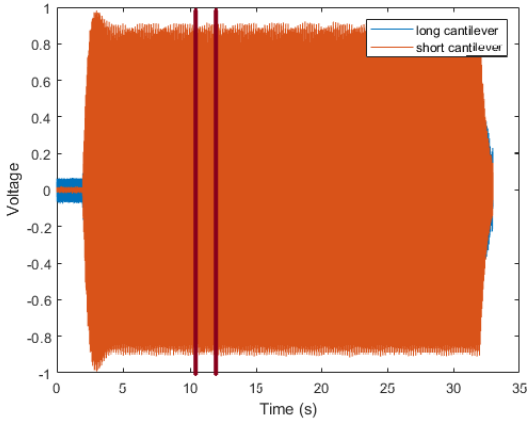

(a) **Uncoupled mechanism, simultaneous sine**

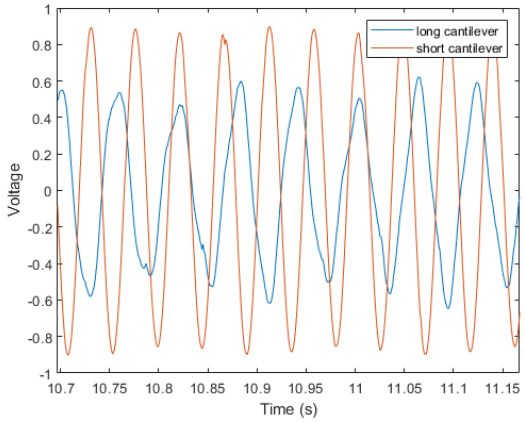

(b) **Transient dynamic behaviour section of graph (a).**

Figure C.8

A waveform can be observed in the voltage response of the uncoupled mechanisms in all figures. The same phenomenon can not be observed in the coupled mechanism responses. The expectation is that this is caused by the limited virtual stiffness of the stage. So the dynamics of the mounted mechanism influence the dynamics of the shaker, which causes the mechanism to not reach a true steady-state vibration mode but instead it keeps fluctuating. This makes if quite difficult to calculate the mean power output over a limited timeframe since also the constantly changing amplitude has to be taken into account.

D

Simulation

In the early stages of this research an effort was made to accurately simulate the dynamic behaviour of the two different mechanisms. The advantage of making such a simulation is that it is more straightforward to research dynamic behaviour over a wide array of different system parameters such as mass or dimensions. Only using an experimental model this process would be quite expensive and time consuming. Two different methods were attempted to build a functioning model, mimicking the physical model.

D.1. Simulink

The first attempt was building a model in Simulink. SimScape building blocks were used to model the hardware. This environment was chosen because it closely resembles building a physical model, using the different parts as building blocks and constraining the interaction between these parts using links. Another advantage using this environment is that it is very easy to experiment with small changes in the model without having to recalculate the governing equations of the system. The building blocks allow the user to pass the relevant parameters, like dimensions and damping coefficient.

In the next two pages the Simulink block schemes are shown. The general structure for the coupled mechanism is as follows: There is a sliding joint between the fixed world and the first cantilever. The sliding joint constraints five DOFs only allowing one DOF which represents the input vibration. The cantilevers are build using 'Flexible rectangular beam' blocks, which allow the user to input mechanical properties like dimensions, stiffness, damping and number of elements the beam consists of. There is a 'Mass' block rigidly connected to the cantilever. The user can input dimensions and inertia to this block. Then the second cantilever is connected to the mass block using a rigid transform and the second proof mass is connected to the second cantilever. To get usable data out of the model a transform sensor is fitted to both the first and second proof mass blocks, and both the rotation and translation boxes are checked. This allows the relevant data to be saved.

The model for the uncoupled mechanism is a bit different. The first part looks a lot like the coupled mechanism but two flexible beam blocks are connected to the first sliding joint which in turn is connected to the fixed world. The two flexible beam blocks have different parameters for their dimensions. Simulink also provides a graphical interface in the Matlab environment which look like figures D.1a and D.1b.

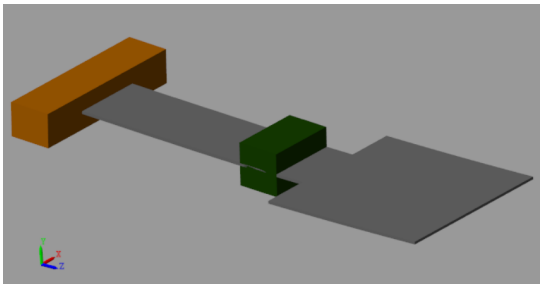

(a) **Graphical interface of Simulink model of coupled mechanism.**

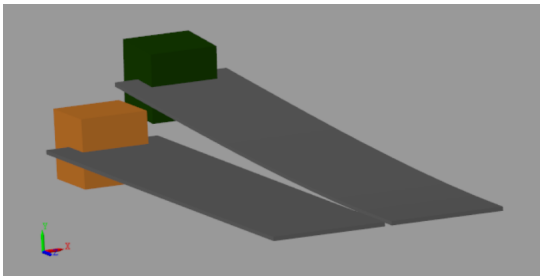

(b) **Graphical interface of Simulink model of uncoupled mechanism.**

Figure D.1

A peculiar effect of this model is even though the frequency response plots of the coupled models seem to match between one another, when excited by a increasing frequency sweep and when doing a bode analysis. Indicating the dynamic response of the model seems to match the physical model, there is a very pronounced difference between the response when excited with a test signal as used in the main thesis body. This can be seen in figure

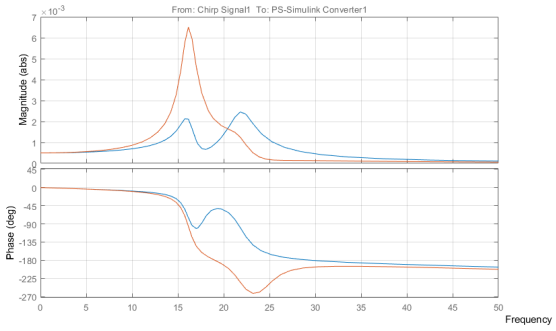

(a) **Bode plot of coupled mechanism, generated through Simulink model.**

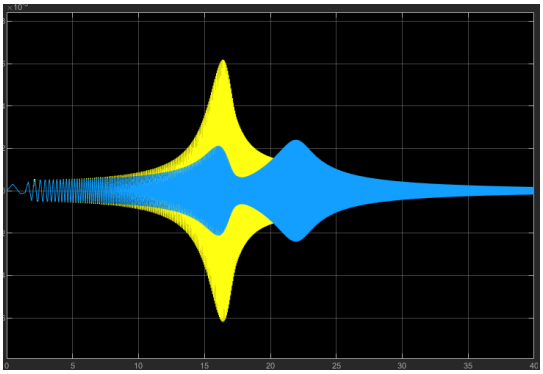

(b) **Dynamic frequency response of coupled mechanism, generated with frequency sweep in Simulink model.**

Figure D.2

When comparing the dynamic response of the physical coupled mechanism to the coupled mechanism model in Simulink, the difference is evident. There is a stark difference between the two responses as can be seen in figure D.3a and D.3b. The damping of of another order of magnitude which makes any comparison between the two impossible. It turned out the type of damping which was chosen for the Simulink model, a proportional damping, was not adequate to describe the damping characteristic of a flexible cantilever beam. In the end it was decided not to continue this line of research using the Simulink model as the model would need to be build from the ground up again costing too much time. This also means that no parametric study into the model parameters is done as the has not reached a level of fidelity needed to be able to get reliable readings.

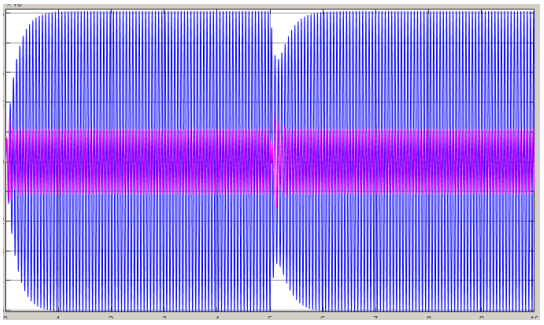

(a) **Simulink simulation of uncoupled mechanism with 90°phaseshift input vibration.**

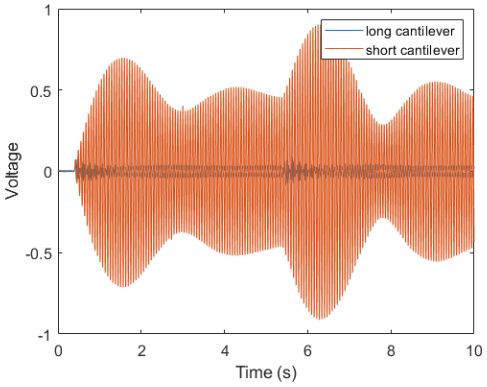

(b) **Experimental data of uncoupled mechanism with 90°phaseshift input vibration.**

Figure D.3

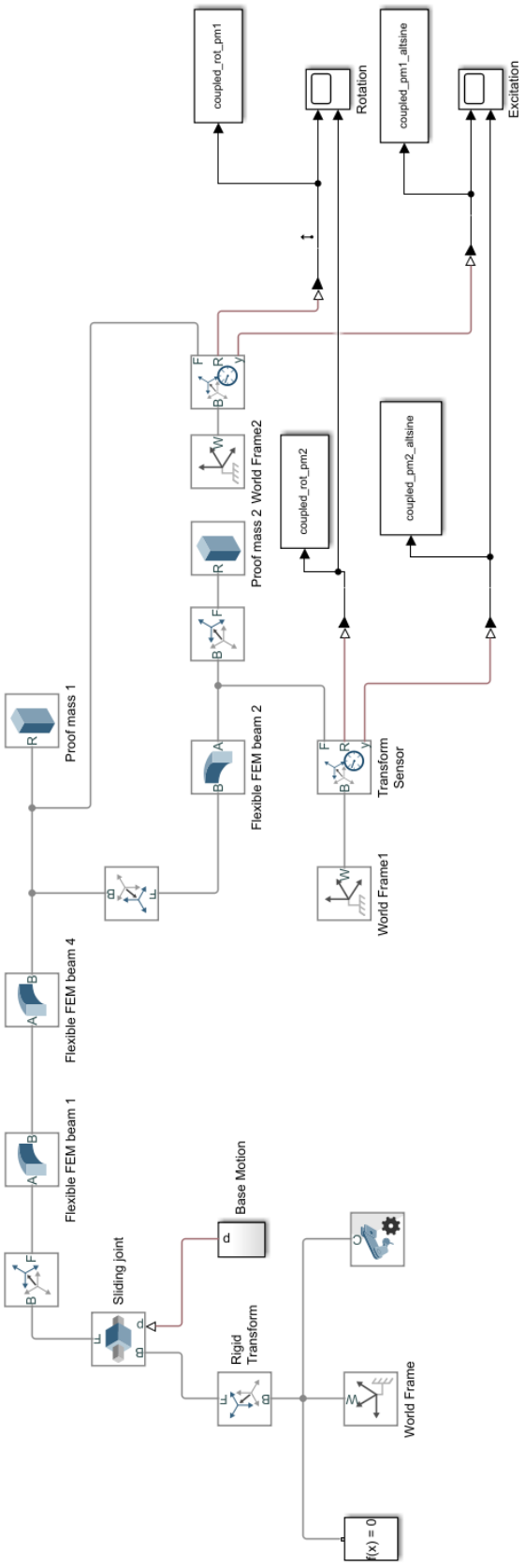

Figure D.4: **Overview of Simulink model of coupled mechanism.**

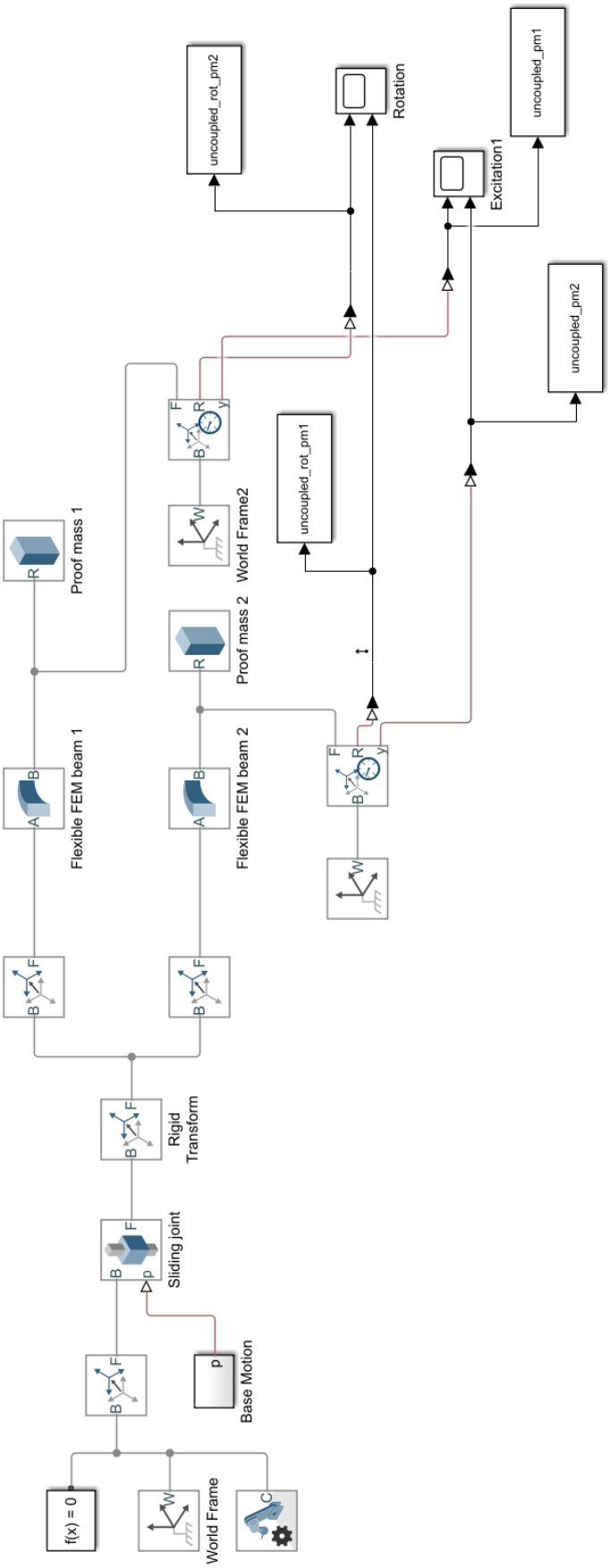

Figure D.5: **Overview of Simulink model of coupled mechanism.**

Bibliography

[1] No Title, 2018. URL https://www.aliexpress.com/i/32965733288.html.

[2] Renewables 2020 – Analysis - IEA, 2020. URL https://www.iea.org/reports/renewables-2020.

[3] No Title, 2020. URL https://www.sciencemag.org/news/2020/05/new-solar-panels-suck-water-air-cool-themselves-down.

[4] Xiaoling Bai, Yumei Wen, Ping Li, Jin Yang, Xiao Peng, and Xihai Yue. Multi-modal vibration energy harvesting utilizing spiral cantilever with magnetic coupling. *Sensors and Actuators, A: Physical*, 209: 78–86, mar 2014. ISSN 09244247. doi: 10.1016/j.sna.2013.12.022.

[5] S. P. Beeby, M. J. Tudor, and N. M. White. Energy harvesting vibration sources for microsystems applications. *Measurement Science and Technology*, 17(12):R175, dec 2006. ISSN 13616501. doi: 10.1088/0957-0233/17/12/R01. URL https://iopscience.iop.org/article/10.1088/0957-0233/17/12/R01https://iopscience.iop.org/article/10.1088/0957-0233/17/12/R01/meta.

[6] S. P. Beeby, R. N. Torah, M. J. Tudor, P. Glynne-Jones, T. O'Donnell, C. R. Saha, and S. Roy. A micro electromagnetic generator for vibration energy harvesting. *Journal of Micromechanics and Microengineering*, 17(7):1257–1265, jul 2007. ISSN 09601317. doi: 10.1088/0960-1317/17/7/007.

[7] T.W.A. Blad and N. Tolou. On the efficiency of energy harvesters: a classification of dynamics in miniaturized generators under low-frequency excitation. *Sagepub*, pages 1–15, 2018. doi: 10.1177/ToBeAssigned. URL http://arxiv.org/abs/1508.04886.

[8] Vinod R. Challa, M. G. Prasad, and Frank T. Fisher. A coupled piezoelectric-electromagnetic energy harvesting technique for achieving increased power output through damping matching. *Smart Materials and Structures*, 18(9):095029, aug 2009. ISSN 09641726. doi: 10.1088/0964-1726/18/9/095029. URL https://iopscience.iop.org/article/10.1088/0964-1726/18/9/095029https://iopscience.iop.org/article/10.1088/0964-1726/18/9/095029/meta.

[9] Sijun Du, Yu Jia, Chun Zhao, Shao Tuan Chen, and Ashwin A. Seshia. Real-world evaluation of a self-startup SSHI rectifier for piezoelectric vibration energy harvesting. *Sensors and Actuators, A: Physical*, 264:180–187, sep 2017. ISSN 09244247. doi: 10.1016/j.sna.2017.07.050.

[10] Li Jiao Gong, Qiao Sheng Pan, Wei Li, Gang Yi Yan, Yong Bin Liu, and Zhi Hua Feng. Harvesting vibration energy using two modal vibrations of a folded piezoelectric device. *Applied Physics Letters*, 107(3), jul 2015. ISSN 00036951. doi: 10.1063/1.4927331.

[11] Jacopo Iannacci, Guido Sordo, Enrico Serra, and Ulrich Schmid. A novel MEMS-based piezoelectric multi-modal vibration energy harvester concept to power autonomous remote sensing nodes for Internet of Things (IoT) applications. *2015 IEEE SENSORS - Proceedings*, pages 1–4, 2015. doi: 10.1109/ICSENS.2015.7370550.

[12] Chang Il Kim, Yong Ho Jang, Young Hun Jeong, Young Jin Lee, Jeong Ho Cho, Jong Hoo Paik, and Sahn Nahm. Performance enhancement of elastic-spring-supported piezoelectric cantilever generator by a 2-degree-of-freedom system. *Applied Physics Express*, 5(3):3–6, 2012. ISSN 18820778. doi: 10.1143/APEX.5.037101.

[13] Jae Eun Kim. On the equivalent mass-spring parameters and assumed mode of a cantilevered beam with a tip mass. *Journal of Mechanical Science and Technology*, 31(3):1073–1078, mar 2017. ISSN 1738494X. doi: 10.1007/s12206-017-0206-1. URL https://link.springer.com/article/10.1007/s12206-017-0206-1.

[14] Miles R. Larkin and Yonas Tadesse. Characterization of a rotary hybrid multimodal energy harvester. In *Active and Passive Smart Structures and Integrated Systems 2014*, volume 9057, page 90570U. SPIE, apr 2014. doi: 10.1117/12.2045271.

[15] S. Leadenham and A. Erturk. Nonlinear M-shaped broadband piezoelectric energy harvester for very low base accelerations: Primary and secondary resonances. *Smart Materials and Structures*, 24(5), may 2015. ISSN 1361665X. doi: 10.1088/0964-1726/24/5/055021.

[16] Huicong Liu, You Qian, and Chengkuo Lee. A multi-frequency vibration-based MEMS electromagnetic energy harvesting device. *Sensors and Actuators, A: Physical*, 204:37–43, 2013. ISSN 09244247. doi: 10.1016/j.sna.2013.09.015. URL http://dx.doi.org/10.1016/j.sna.2013.09.015.

[17] Huicong Liu, Tao Chen, Lining Sun, and Chengkuo Lee. An electromagnetic MEMS energy harvester array with multiple vibration modes. *Micromachines*, 6(8):984–992, 2015. ISSN 2072666X. doi: 10.3390/mi6080984.

[18] Huicong Liu, Tao Chen, Lining Sun, and Chengkuo Lee. An electromagnetic MEMS energy harvester array with multiple vibration modes. *Micromachines*, 6(8):984–992, 2015. ISSN 2072666X. doi: 10.3390/mi6080984.

[19] Robert B. MacCurdy, Timothy Reissman, and Ephrahim Garcia. Energy management of multi-component power harvesting systems. In Mehdi Ahmadian, editor, *Active and Passive Smart Structures and Integrated Systems 2008*, volume 6928, page 692809. SPIE, mar 2008. ISBN 9780819471147. doi: 10.1117/12.776545. URL http://proceedings.spiedigitallibrary.org/proceeding.aspx?doi=10.1117/12.776545.

[20] Venkateswara Sarma Mallela, V. Ilankumaran, and Srinivasa N. Rao. Trends in cardiac pacemaker batteries. *Indian Pacing and Electrophysiology Journal*, 4(4):201–212, oct 2004. ISSN 09726292. URL www.ipej.org201.

[21] By Paul D Mitcheson, Member Ieee, Eric M Yeatman, Senior Member Ieee, G Kondala Rao, Student Member Ieee, Andrew S Holmes, Member Ieee, Tim C Green, and Senior Member Ieee. Energy Harvesting From Human and MachineMotion for Wireless Electronic Devices. 96(9):1457–1486, 2008.

[22] Son D. Nguyen and Einar Halvorsen. Nonlinear springs for bandwidth-tolerant vibration energy harvesting. *Journal of Microelectromechanical Systems*, 20(6):1225–1227, dec 2011. ISSN 10577157. doi: 10.1109/JMEMS.2011.2170824.

[23] Denis Pombriant. No Title, 2019. URL https://denispombriant.medium.com/the-21st-century-version-of-hydropower-926ac8991d45.

[24] J. M. Ramírez, C. D. Gatti, S. P. Machado, and M. Febbo. A multi-modal energy harvesting device for low-frequency vibrations. *Extreme Mechanics Letters*, 22:1–7, jul 2018. ISSN 23524316. doi: 10.1016/j.eml.2018.04.003.

[25] R. Ramlan, M. J. Brennan, B. R. MacE, and I. Kovacic. Potential benefits of a non-linear stiffness in an energy harvesting device. *Nonlinear Dynamics*, 59(4):545–558, mar 2010. ISSN 0924090X. doi: 10.1007/s11071-009-9561-5.

[26] Shad Roundy. On the effectiveness of vibration-based energy harvesting. *Journal of Intelligent Material Systems and Structures*, 16(10):809–823, 2005. ISSN 1045389X. doi: 10.1177/1045389X05054042.

[27] S. M. Shahruz. Design of mechanical band-pass filters for energy scavenging. *Journal of Sound and Vibration*, 292(3-5):987–998, may 2006. ISSN 10958568. doi: 10.1016/j.jsv.2005.08.018.

[28] Wei Jiun Su, Jean Zu, and Yang Zhu. Design and development of a broadband magnet-induced dual-cantilever piezoelectric energy harvester. *Journal of Intelligent Material Systems and Structures*, 25(4):430–442, mar 2014. ISSN 1045389X. doi: 10.1177/1045389X13498315.

[29] Shilong Sun and Peter W. Tse. Design and performance of a multimodal vibration-based energy harvester model for machine rotational frequencies. *Applied Physics Letters*, 110(24), jun 2017. ISSN 00036951. doi: 10.1063/1.4986477.

[30] Lihua Tang and Yaowen Yang. A multiple-degree-of-freedom piezoelectric energy harvesting model. *Journal of Intelligent Material Systems and Structures*, 23(14):1631–1647, sep 2012. ISSN 1045389X. doi: 10.1177/1045389X12449920.

[31] R. M. Toyabur, M. Salauddin, and Jae Y. Park. Design and experiment of piezoelectric multimodal energy harvester for low frequency vibration. *Ceramics International*, 43:S675–S681, aug 2017. ISSN 02728842. doi: 10.1016/j.ceramint.2017.05.257.

[32] R. M. Toyabur, M. Salauddin, and Jae Y. Park. Design and experiment of piezoelectric multimodal energy harvester for low frequency vibration. *Ceramics International*, 43:S675–S681, aug 2017. ISSN 02728842. doi: 10.1016/j.ceramint.2017.05.257.

[33] Deepesh Upadrashta and Yaowen Yang. Trident-Shaped Multimodal Piezoelectric Energy Harvester. *Journal of Aerospace Engineering*, 31(5):1–9, 2018. ISSN 08931321. doi: 10.1061/(ASCE)AS.1943-5525.0000899.

[34] Connel B. Williams and Rob B. Yates. Analysis of a micro-electric generator for microsystems. *Sensors and Actuators, A: Physical*, 52(1-3):8–11, mar 1996. ISSN 09244247. doi: 10.1016/0924-4247(96)80118-X.

[35] Hao Wu, Lihua Tang, Yaowen Yang, and Chee Kiong Soh. A compact 2 degree-of-freedom energy harvester with cut-out cantilever beam. *Japanese Journal of Applied Physics*, 51(4 PART 1):2–5, 2012. ISSN 00214922. doi: 10.1143/JJAP.51.040211.

[36] Hao Wu, Lihua Tang, Yaowen Yang, and Chee Kiong Soh. A novel two-degrees-of-freedom piezoelectric energy harvester. In *Journal of Intelligent Material Systems and Structures*, volume 24, pages 357–368, feb 2013. doi: 10.1177/1045389X12457254.

[37] Zhao Xiao, Tong Qing Yang, Ying Dong, and Xiu Cai Wang. Energy harvester array using piezoelectric circular diaphragm for broadband vibration. *Applied Physics Letters*, 104(22), jun 2014. ISSN 00036951. doi: 10.1063/1.4878537.